OPEN ACCESS

Original research

Dominant negative mutation in oxalate transporter *SLC26A6* associated with enteric hyperoxaluria and nephrolithiasis

Nicolas Cornière,[1,2] R Brent Thomson,[3] Stéphanie Thauvin,[4] Bruno O Villoutreix,[5] Sophie Karp,[3] Diane W Dynia,[3] Sarah Burlein,[3] Lennart Brinkmann,[3] Alaa Badreddine ,[2] Aurélie Dechaume,[2] Mehdi Derhourhi,[2] Emmanuelle Durand,[2] Emmanuel Vaillant,[2] Philippe Froguel,[2] Régine Chambrey,[2,4] Peter S Aronson ,[3] Amélie Bonnefond,[2] Dominique Eladari [1,2]

► Additional supplemental material is published online only. To view, please visit the journal online (http://dx.doi.org/10.1136/jmedgenet-2021-108256).

[1]Department of Precision Médicine for Metabolic and Renal Diseases, CHU Amiens Picardie, Université de Picardie Jules Verne, Amiens, France
[2]UMR1283, INSERM; CNRS; University of Lille, Lille, Hauts de France, France
[3]Department of Internal Medicine, Yale University School of Medicine, New Haven, Connecticut, USA
[4]Plateau de Recherche ODHIR, AURAR, Saint-Gilles-les-Bains, Réunion
[5]UMR 1141, INSERM, Paris, Île-de-France, France

Correspondence to
Professor Dominique Eladari, CHU Amiens Picardie, Université de Picardie Jules Verne, Amiens, France;
dominique.eladari@inserm.fr

NC and RBT are joint first authors.
AB and DE are joint senior authors.

Received 11 October 2021
Accepted 11 January 2022
Published Online First 3 February 2022

Check for updates

To cite: Cornière N, Thomson RB, Thauvin S, *et al*. *J Med Genet* 2022;**59**:1035–1043.

ABSTRACT

Background Nephrolithiasis (NL) is a complex multifactorial disease affecting up to 10%–20% of the human population and causing a significant burden on public health systems worldwide. It results from a combination of environmental and genetic factors. Hyperoxaluria is a major risk factor for NL.

Methods We used a whole exome-based approach in a patient with calcium oxalate NL. The effects of the mutation were characterised using cell culture and in silico analyses.

Results We identified a rare heterozygous missense mutation (c.1519C>T/p.R507W) in the *SLC26A6* gene that encodes a secretory oxalate transporter. This mutation cosegregated with hyperoxaluria in the family. In vitro characterisation of mutant SLC26A6 demonstrated that Cl^--dependent oxalate transport was dramatically reduced because the mutation affects both SLC26A6 transport activity and membrane surface expression. Cotransfection studies demonstrated strong dominant-negative effects of the mutant on the wild-type protein indicating that the phenotype of patients heterozygous for this mutation may be more severe than predicted by haploinsufficiency alone.

Conclusion Our study is in line with previous observations made in the mouse showing that *SLC26A6* inactivation can cause inherited enteric hyperoxaluria with calcium oxalate NL. Consistent with an enteric form of hyperoxaluria, we observed a beneficial effect of increasing calcium in the patient's diet to reduce urinary oxalate excretion.

INTRODUCTION

Nephrolithiasis (NL) is the second most frequent renal disease after hypertension affecting up to 10% of individuals worldwide, and in nearly all countries, its prevalence and incidence are reported to be rising.[1] NL is highly recurrent and is a major cause of patient pain, disability and lost working days. It is also associated with increased risks of cardiovascular disease, bone demineralisation and fractures, chronic kidney disease and end-stage renal disease.[2–4]

The vast majority of kidney stones is composed of calcium oxalate.[5] Even a small increase in urinary oxalate markedly promotes calcium oxalate crystal formation,[6–8] and hence, hyperoxaluria is a major risk factor for kidney stones.[7] The oxalate found in urine is either from exogenous or endogenous origin. Dietary oxalate, which accounts for almost 50% of the oxalate excreted in urine,[9] is abundantly present in plant and animal sources, absorbed by the gut and excreted unchanged in the urine.[9] In addition, endogenous oxalate production occurs in the liver resulting from the metabolism of glyoxylate.[10 11] Primary hyperoxaluria (PH) is an inherited autosomal recessive metabolic disorder that results from increased endogenous oxalate production, whereas secondary hyperoxaluria is acquired and caused by excessive intake of dietary oxalate or of oxalate precursors or by factors that can increase net oxalate absorption by the gastrointestinal tract (eg, low calcium diet, lipid malabsorption and abnormal microbiome). Therefore, identification of the potential mechanisms leading to hyperoxaluria is an important step to optimise care and treatment of oxalate-dependent NL.

In mice, ablation of the oxalate transporter SLC26A6 causes a defect in intestinal oxalate secretion that results in increased net absorption of dietary oxalate,[12] leading to hyperoxaluria and calcium oxalate NL.[12 13] This observation supports the possibility that an additional type of inherited hyperoxaluria might exist in human patients due to mutations leading to defective intestinal oxalate secretion, thereby resulting in enhanced net intestinal absorption of oxalate. Four studies have assessed the impact of *SLC26A6* variants in humans.[14–17] However, these studies either reported no association of *SLC26A6* variants with hyperoxaluria or with NL,[14–16] or reported mutations that disrupt a complex between SLC26A6 and the citrate transporter NaDC-1 thereby causing hypocitraturia as a risk factor for NL.[17] Therefore, no rare human *SLC26A6* variant contributing to hyperoxaluria has been reported so far.

Here, we report a family in which a rare heterozygous missense mutation in the *SLC26A6* gene is associated with hyperoxaluria and recurrent bilateral

calcium oxalate NL. In vitro characterisation of the mutant demonstrated that the mutation leads to defective membrane expression and oxalate transport activity with evidence of a dominant negative effect on wild-type (WT) transporter. We conclude that rare, deleterious mutations in *SLC26A6* gene are a possible cause of inherited hyperoxaluria and therefore can promote NL in humans.

CONCISE METHODS

A detailed description of material and methods is available as online supplemental information.

Patients testing

Biochemical and hormone measurements were performed using standard techniques as detailed in online supplemental materials.

Participants from UK Biobank

We analysed up to 200 619 samples with available exome sequencing data. This research is part of UK Biobank research application #67 575. The strategy used in this study to identify patients with kidney stones is reported in online supplemental materials.

DNA sequence analyses

The DNA proband was assessed through whole-exome sequencing at the genotyping platform of the European Genomic Institute for Diabetes (Lille, France). For this purpose, we used the Human Core Exome EF Multiplex Complete kit (Twist Bioscience) in combination with Illumina next-generation sequencing.

The *SLC26A6* mutation was confirmed in the proband through Sanger sequencing, and then assessed in the family members. Primer sequences and PCR conditions are available on request. Fragments were sequenced in both directions and subsequently analysed using the 3730xl DNA Analyzer (Applied Biosystems). Electropherogram reads were assembled and examined using the SeqScape software (Applied Biosystems).

Detection of variants in UK Biobank

We used exome data from pVCF format (field #23 156). Only variants with a coverage higher than 10 reads and quality Genotype quality (GQ) score higher than 20 were kept for further analyses. Annotation of variants was done using the Ensembl Variant Effect Predictor tool V.103 (RefSeq).

In silico analyses of the effects of the p.R507W mutation on Slc26a6 protein

A structural model of human SLC26A6 was developed using the experimental structure of the mouse SLC26A9 homodimer anion transporter as structural template.[18] Different structural bioinformatics approaches were used to investigate the model structure and the amino acid replacement including the computations of ΔΔG values between the WT and the variant proteins. The different approaches used and additional structural analyses are reported in the online supplemental material section.

SLC26A6 expression constructs

An HA-tagged wild-type human SLC26A6 cDNA expression construct (HA-WT)[19] was used to generate HA-tagged and myc-tagged p.R507W human SLC26A6 mutants (HA-MT and *myc*-MT, respectively) with a Q5 site-directed mutagenesis kit (New England Biolabs).

Cell culture and transfections

OKP cells (American Type Culture Collection(ATTC)) were used for all transfection experiments. 1×10^5 OKP cells per well of a 24 wells cell culture dish were reverse transiently transfected with 2 µL of Lipofectamine 2000 (Thermo Scientific) and 0.1–0.25 µg of HA-WT, *myc*-WT or HA-MT cDNA as indicated in the respective figure legend for each experiment. Cells were assayed 72 hours post-transfection.

Cell surface biotinylation

OKP cells were surface biotinylated 72 hours post-transfection as described previously.[19] Membranes were probed with a rabbit anti-SLC26A6 polyclonal antibody[19] (R29; 1:50 000 dilution), a rabbit anti-HA polyclonal antibody (71–5500; 1:250 dilution; Thermo Scientific) or a mouse anti-*myc* monoclonal antibody (R950-25; 1:5000 dilution; Thermo Scientific). Primary antibody labelling was detected with either a donkey antirabbit or a donkey antimouse Horse Radish Peroxydase (HRP-labelled secondary antibody (711-035-152 and 715-035-150 respectively; 1:20 000 dilution; Jackson ImmunoResearch),[19] visualised by enhanced chemiluminescence (Clarity Western ECL Substrate; Bio-Rad) and recorded on film.

Coimmunoprecipitation

Transfected OKP cells were cultured for 72 hours prior to solubilisation with 1% digitonin. *myc*-tagged WT SLC26A6 was immunoprecipitated from OKP cell detergent lysates with the anti-*myc* antibody R950-25 (Thermo; 5 µg IgG/mL lysate). Immunoprecipitates were captured with Protein G Sepharose Fast Flow (Sigma P3296), and then Sepharose beads were washed extensively with a series of normal and high salt washes to reduce non-specific binding. Immunoprecipitates were released from sepharose beads by incubation with 2× Sodium Dodecyl Sulfate (SDS)-PAGE sample buffer containing 100 mM dithiothreitol (DTT) for 2 min at 100°C. The immunoprecipitates were subjected to SDS-PAGE, transferred to a polyvinylidene fluoride (PVDF membrane and then analysed by western blot with antibodies directed against the HA-epitope and *myc*-epitope tags (71–5500 and R950-25 antibodies, respectively).

Cl^--dependent ^{14}C-oxalate uptake

See reference ref 19 for a detailed description of the rationale and methodology behind the assessment of Cl^--gradient dependent ^{14}C-oxalate uptake mediated by the SLC26A6 expression constructs (HA-WT and HA-MT) when transfected into OKP cells. Briefly, uptakes were performed for each transfection condition in the presence and absence of an outwardly directed chloride gradient to provide an estimate of the proportion of the total ^{14}C-oxalate cell uptake that was specifically chloride dependent. Uptakes were also performed in untransfected cells (exposed to transfection reagent alone) to provide an estimate of background levels of endogenous chloride-dependent ^{14}C-oxalate uptake. The background values were then subtracted from the values in transfected cells to determine the level of chloride-dependent ^{14}C-oxalate uptake that is directly and solely attributable to the activity of the transfected SLC26A6 expression constructs.

Statistics

Data values are presented as mean±SEM. Statistical significance was evaluated by unpaired two-tailed Student's t-test (GraphPad Prism).

RESULTS

Primary clinical data of the proband

The patient is a late adolescent woman from non-consanguineous parents. She has a personal history of Hashimoto's thyroiditis diagnosed during her early adolescence and replacement with L-thyroxine. She had her first renal colic during her early adolescence. Since then, she has had recurrent renal colic (>20) and passed multiple kidney stones. Abdominal CT and ultrasound detected multiple and bilateral stones without nephrocalcinosis (online supplemental figure S1). A spontaneously evacuated kidney stone was analysed by infrared spectrometry revealing a composition of calcium oxalate monohydrate (~80% whewellite) suggesting that NL is oxalate dependent. Biochemical analyses, performed in the absence of any treatment and 2 months after her last renal colic (table 1), identified the presence of frank hyperoxaluria (733 µmol/day, N: 40–330), which was confirmed on a second independent urine sampling (800 µmol/day, N: 40–330). Adequacy of urine collection was attested by measuring the daily excretion of creatinine (0.16 mmol/kg/day, N: 0.12–0.19). Interview with a dietitian excluded excessive intake in oxalate-rich aliments (~50 mg/day) and revealed very low calcium intake (~400 mg/day). The patient had no history of bowel disease or diarrhoea and showed no sign of malabsorption. Table 1 also showed no biological evidence of malabsorption. Kidney stone-causing conditions like vitamin D excess or primary systemic disease (eg, primary hyperparathyroidism or renal leak of phosphate) were excluded. The calcium-loading test detected increased digestive absorption of calcium as evidenced by the increased delta between postcalcium load calciuria and fasting calciuria. However, the patient did not exhibit hypercalciuria. The only other risk factor for NL was very mild hypocitraturia (1.18 mmol/24 hours, N>1.67). The patient exhibited no extrarenal symptoms or biological abnormalities suggesting systemic oxalosis, and renal function appeared normal.

Table 1 Characteristics, blood and urine analyses and calcium-loading test of the patients

	Proband	Father	Normal range (95% CI)
BSA (m^2)	1.55	1.69	
BMI (kg/m^2)	23.9	23.9	
Blood analyses			
Plasma (Na^+) (mM)	141	137	135 to 145
Plasma (K^+) (mM)	4.0	4.6	3.3 to 5.1
Plasma (Cl^-) (mM)	106	104	95 to 105
Plasma (HCO_3^-) (mM)	21	27	21 to 29
Serum (creatinine) (µM)	42	93	
eGFR (CKD-EPI; mL/min/1.73 m^2)	143	78	
Hb (g/dL)	13.8	N.A.	12.0 to 16.0
Serum iron (µM)	14.1	N.A.	6.6 to 26.0
Serum ferritin µg/L	29.0	N.A.	15 to 150
Transferrin saturation coefficient (%)	21.0	N.A.	15 to 35
Serum transferrin (g/L)	2.74	N.A.	2.0 to 3.6
Prothrombin time (%)	91	N.A.	70 to 100
Serum albumin	47.2	N.A.	35.0 to 52.0
Calcium-loading test			
Fasting ionised p(Ca^{2+})(mM)	1.16	1.20	1.15 to 1.32
Ionised p(Ca^{2+}) after calcium loading (mM)	1.22	1.22	1.15 to 1.32
Fasting Pi (mM)	1.02	0.99	0.81 to 1.45
Fasting TmPi/GFR (mM)	1.01	0.79	0.76 to 1.62
Fasting (Mg^{2+}) (mM)	0.93	0.97	0.66 to 0.99
Fasting 25(OH) vit. D (nM)	**51***	82	75 to 130
1,25(OH)2 vitamin D (pM)	157	156	43 to 168
Fasting (PTH) (ng/L)	48	51	15 to 65
(PTH) after calcium loading (ng/L)	27	31	15 to 65
Fasting urinary Ca^{2+} (mM/mM creatinine)	0.29	0.26	0.04 to 0.37
Δurinary Ca^{2+} after calcium loading (mM/mM creatinine)	**1.55***	0.48	0.22 to 0.54
24-hour urine			**Usual range**
Urine output (L/day)	2.96	4.01	
Creatinine (mmol/kg/day)	0.16	0.20	M: 0.17 to 0.23
			F: 0.12 to 0.19
Na^+ (mmol/day)	109	130	
K^+ (mmol/day)	50	115	
Urea (mmol/day)	251	462	
Ca^{2+} (mmol/day)	2.96	5.3	M<7.25, F<6.5
Citrate (mmol/day)	**1.18***	2.73	>1.67
Oxalate (µmol/day)	**733***	**520***	40 to 330
Urate (mmol/day)	2.4	4.7	1.8 to 4.8
Proteines (g/day)	0.15	0.15	<0.15
Albumin (mg/day)	18	17	<30
Fasting urine			
Fasting (creatinine) (mM)	2.5	1.94	<10 mM
pH	5.65	7.08	

BMI, Body Mass Index; BSA, Body Surface Area; CKD-EPI, Chronic Kidney Disease Epidemiology collaboration equation; eGFR, estimated GFR; Hb, hemoglobin; N.A., not available; pH, potential of Hydrogen; Pi, inorganic phosphate; TmPi/GFR, renal phosphate tubular reabsorption threshold.

Identification of a rare heterozygous missense mutation in Slc26a6

Through whole-exome sequencing of the proband's DNA, we investigated rare coding variants of potential interest with minor allele frequency below 0.1% in the Genome Aggregation Database (GnomAD V.2.1.1) in a list of genes or candidate genes linked with NL (online supplemental table 1). We did not find any pathogenic or likely pathogenic variant according to the criteria of the American College of Medical Genetics and Genomics.[20] No pathogenic or likely pathogenic variant or variant of unknown significance was detected in the three genes involved in PH. However, we found a rare heterozygous variant of unknown significance located in the 13th coding exon of *SLC26A6* (NM_022911.2: c.1519C>T; p.R507W). SLC26A6 encodes an oxalate transporter involved in hyperoxaluria and NL based on mouse knockout studies.[12 13] According to GnomAD (V.2.1.1), *SLC26A6* is intolerant to loss-of-function variation with an observed/expected score of 0.65 (0.48–0.91), and the p.R507W mutation is very rare, as it has been found in only 5 out of 280 674 alleles reported in GnomAD (in Europeans and South Asians). According to SIFT, Mutation Taster and PolyPhen-2 (HumDiv), the p.R507W mutation was predicted to be deleterious, disease causing and damaging, respectively.[21–23]

Human SLC26A6 residue p.R507 was found fully conserved in an interspecies comparison. The conservation of this residue was also very high in this family of proteins (ie, the score at position 507 was equal to 8, the maximum is 9, via the Consurf server). We then built a homology model using as experimental template the mouse Slc26a9 homodimer anion transporter tridimensional (3D structure (figure 1). The modelling was possible as the overall sequence identity between the two proteins is around 40% (see online supplemental materials).

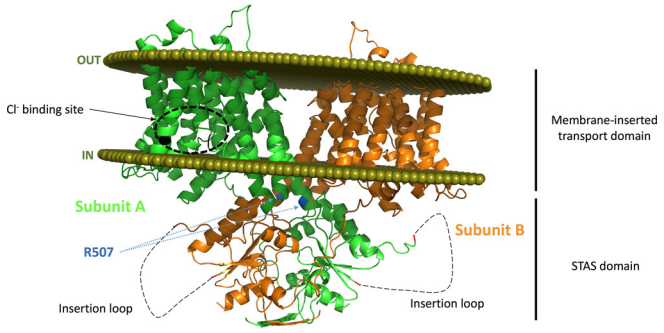

Figure 1 In silico analysis of the putative effects of the R507W substitution on the SLC26A6 protein structure. The two subunits are presented with one subunit coloured in green and the other in orange (cartoon representation). The olive spheres represent the boundary of the lipid bilayer as computed with the PPM server. A zone predicted to interact with the Cl^- ion as proposed in the mouse SLC26A9 experimental structure is highlighted by a black dashed circle in subunit a for orientation. R507 residues of both subunits are flagged and coloured in blue; this residue is located on the last helix of the transmembrane domain 22 residues prior to the beginning of the Sulfate Transporter Antagonist of anti-Sigma factor (STAS domain. The insertion loop that could not be built is shown as a dashed line. The mutation is expected to destabilise the protein and to impede optimal insertion into the lipid bilayer.

The human SLC26A6 model structure positioned into a membrane is shown in figure 1. p.R507 is located on the C-terminal side of the last transmembrane helix, prior to the STAS domain. The region of p.R507 is predicted to be essentially rigid (PredyFlexy computation) and thus not very tolerant to the p.R507W substitution, which was predicted to likely perturb correct interaction with the membrane. The details of our in silico analyses are provided as online supplemental materials.

Family investigation of the Slc26a6 p.R507W mutation

Since the *SLC26A6* mutation was potentially pathogenic, both parents of the proband were assessed. Sanger sequencing identified the same heterozygous *SLC26A6* mutation in the father, while the mother was WT (online supplemental figure S2). The mother had no personal or familial history of kidney stones and exhibited normal levels of urinary oxalate (250 µmol/day, N: 40–330).

Even though the father did not report any renal colic, biochemical analyses revealed that he also had hyperoxaluria (520 µmol/day, N: 40–330). The calcium loading test was strictly normal, and no other risk factor for NL was identified for the father (table 1). However, we noticed that he exhibited a urine output of almost 4 L/day reflecting a very high-water intake. This high urine output may explain why he never experienced kidney stones. Furthermore, contrasting with the proband, he did not exhibit any hypocitraturia. No other relatives from same family were accessible for medical examination and genetic testing.

Response to medical treatment

We hypothesised that the proband presented with inherited enteric hyperoxaluria due to deficient SLC26A6-mediated oxalate secretion resulting in increased net absorption of dietary oxalate. We advised her to increase drinking water intake in order to reach a urinary output of at least 3 L/day and to systematically add a dairy product to each meal in order to increase her calcium intake up to the recommended daily amounts of 900 mg/day. The latter intervention turned out to be very effective, as urinary oxalate excretion markedly dropped from >700 µmol/day down to ~300 µmol/day on repeated control analyses while the mild hypocitraturia persisted (1.49 mmol/24 hours N<1.67). No other medication was initiated, and NL also dramatically improved, as she has not experienced any recurrence of kidney stones for 2 years of follow-up.

Physiological characterisation of the variant

In order to assess the pathogenicity of the *SLC26A6* p.R507W mutation, we next assessed its effect on protein expression, protein trafficking and chloride-dependent oxalate transport. Under physiological conditions, apical membrane SLC26A6 in epithelial cells mediates oxalate secretion by operating in the direction of exchanging intracellular oxalate for extracellular chloride. However, SLC26A6 can mediate Cl^--oxalate exchange in either direction depending on the direction of the net driving force. We measured Cl^--gradient stimulated ^{14}C-oxalate uptake as a measure of oxalate transport activity mediated by human SLC26A6 transfected into OKP epithelial cells, as in previous studies of SLC26A6 glycosylation mutants.[19] We specifically evaluated the chloride-dependent component of ^{14}C-oxalate uptake that was mediated by the transfected human SLC26A6 expression constructs by correcting for endogenous oxalate transport (see Methods and online supplemental figure S3 for details).

Characterisation of the effect of the p.R507W mutation on expression and function of human SLC26A6 transfected into OKP cells is shown in figure 2. Results are illustrated for three independent experiments in which OKP cells were transfected with identical amounts of cDNA encoding the WT and mutant (MT) transporters. Figure 2A shows immunoblots of total cell lysate and compared transfected cells with an untransfected control lane. Transfection of OKP cells results in expression of a minor band just under 75 kDa and multiple prominent bands >100 kDa. As demonstrated in a previous study, the lower band corresponds in size to nascent unglycosylated SLC26A6, whereas the upper bands correspond to complex-glycosylated SLC26A6.[19] Surface biotinylated SLC26A6 is shown in figure 2B, corresponding in size to the complex-glycosylated forms of SLC26A6. As illustrated by the immunoblots in figure 2A and B and summarised by the densitometry in figure 2C, there was a marked reduction in glycosylated and cell surface expression of the mutant transporter compared with WT. Although these findings indicate that the p.R507W mutation leads to decreased processing and trafficking, and/or increased degradation of the transporter, the qualitative similarity of the western blot molecular weight band profiles of the WT and MT constructs strongly suggests that the mutation does not directly affect the glycosylation of SLC26A6 per se. As shown in figure 2D, chloride-dependent ^{14}C-oxalate uptake mediated by mutant SLC26A6 was also markedly impaired. Of interest, whereas the mutation resulted in approximately a 50% reduction in cell surface expression of SLC26A6 (figure 2C), it led to a disproportionately higher reduction of Cl^--dependent oxalate transport activity of approximately 75%. This suggested that the mutation might affect both the expression and the intrinsic transport capability of SLC26A6.

We therefore next designed an experiment to test directly whether the mutation causes a defect in the intrinsic transport function of SLC26A6 in addition to the defect in net surface expression demonstrated in figure 2. Cells were transfected with 2.5-fold more mutant than WT cDNA with the goal of approximately equalising surface expression of the mutant and

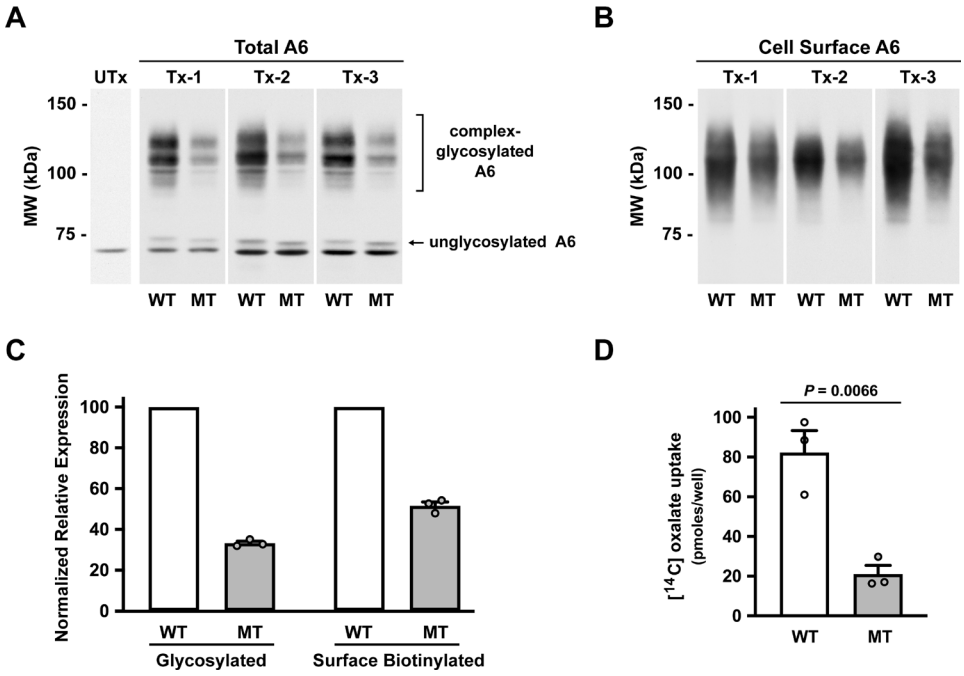

Figure 2 Characterisation of the R507W SLC26A6 mutation in transfected OKP cells. OKP cells were transfected with equivalent amounts (0.1 µg cDNA per well of a 24-well dish) of either wild-type (WT; HA-WT) or mutant (MT; HA-MT) human SLC26A6 cDNA. Cells were assayed 72 hours post-transfection. For each transfection (Tx-1 to 3), uptakes and companion biotinylations were performed in triplicate. Utx, untransfected control. Panels A+B show representative images selected from each transfection. Western blots were probed with the antihuman Slc26a6 polyclonal antibody, R29. Panel A: western analysis of total cell lysates isolated from each transfection condition. Panel B: western analysis of cell surface biotinylatable hA6 from each transfection condition. Panel C: expression levels of total and cell surface biotinylatable hA6. Expression levels were determined by densitometry. To facilitate comparisons between transfections (n=3 independent transfections), MT expression levels for each transfection were normalised to mean densitometry values for the WT densitometry values for each transfection. All WT levels are expressed as 100 (%), and the individual MT values vary accordingly. Panel D: chloride-dependent ^{14}C-oxalate uptake attributable to transfected wild-type (WT; HA-WT) and mutant (MT; HA-MT) Slc26a6. The uptake values are presented as pmoles ^{14}C-oxalate uptake per well of a 24-well plate and are not normalised to levels of expressed protein. WT, wild type; HA-WT, hemagglutinin-tagged wild type; MT, mutant; HA-MT, hemagglutinin-tagged mutant; tx, transfection; Utx, untransfected.

WT transporters. As illustrated by the immunoblots in figure 3A and B and summarised by the densitometry in figure 3C, the protocol achieved roughly equivalent amounts of the glycosylated and surface expressed forms of the mutant and WT transporters. Most importantly, assessment of transport activity normalised to surface expression, as shown in figure 3D, indicated that the p.R507W mutation does indeed cause a marked defect (approximately 50%) in intrinsic transport activity of SLC26A6. The findings of figures 2 and 3 taken together suggest that the 75% defect in transport activity of mutant compared with WT SLC26A6 when equal amounts of cDNA are transfected (figure 2D) results from about a 50% defect in cell surface expression (figure 2C) and a roughly 50% defect in intrinsic transporter activity (figure 3D).

Given that SLC26 family transporters exist as dimers,[18 24] we conducted additional studies to test the possibility of a dominant negative effect of the p.R507W mutation on expression of the WT transporter. Our approach was to assay expression of *myc*-tagged WT SLC26A6 as a function of cotransfection with either HA-tagged WT or HA-tagged mutant transporter. We chose transfection conditions to achieve equivalent expression levels of HA-WT and HA-MT SLC26A6 (online supplemental figure S4). As illustrated by the immunoblots in figure 4A and B, and summarised by the densitometry in figure 4C, coexpression of mutant SLC26A6 caused 70% reduction in glycosylated and cell surface expression of *myc*-tagged WT SLC26A6 compared with coexpression of WT SLC26A6. These results support the possibility that the p.R507W mutation may have a dominant negative effect on expression of the WT transporter so that the hyperoxaluria phenotype of patients heterozygous for this mutation may be more severe than predicted by haploinsufficiency alone.

We next performed a series of WT/MT co-immunoprecipitation studies to verify the association of MT with WT transporter to explain the dominant negative phenotype. OKP cells were cotransfected with *myc*-tagged WT SLC26A6 and either HA-tagged WT SLC26A6 or HA-tagged MT SLC26A6 as described for the experiment outlined in figure 4. The cells were solubilised with 1% digitonin, subjected to immunoprecipitation with an anti-*myc* antibody, and the resulting immunoprecipitates were analysed by SDS-PAGE and western blot with antibodies directed against either the *myc*-tag or the HA-tag (figure 5).

As observed in the previous experiment (figure 4), cotransfection of mutant HA-A6 with wild-type *myc*-A6 led to a dramatic decrease in expression of mature WT *myc*-A6 in both the solubilised lysate (figure 5A) and the companion primary immunoprecipitation (figure 5C). Western analysis of the solubilised lysate with the anti-HA antibody (figure 5B) confirmed that cotransfection with 2.5× HA-MT relative to HA-WT resulted in roughly similar levels of expression of the two HA-tagged SLC26A6 expression constructs. We observed significant coimmunoprecipitation of both wild-type and mutant HA-A6 with the *myc*-tagged WT-A6 (figure 5D). Despite the presence of similar amounts of HA-WT and HA-MT in the initial cell lysates for each experiment (figure 5B), their relative recoveries by coimmunoprecipitation could only reflect, at best, the relative recovery of the primary immunoprecipitated binding partner (*myc*-WT). If

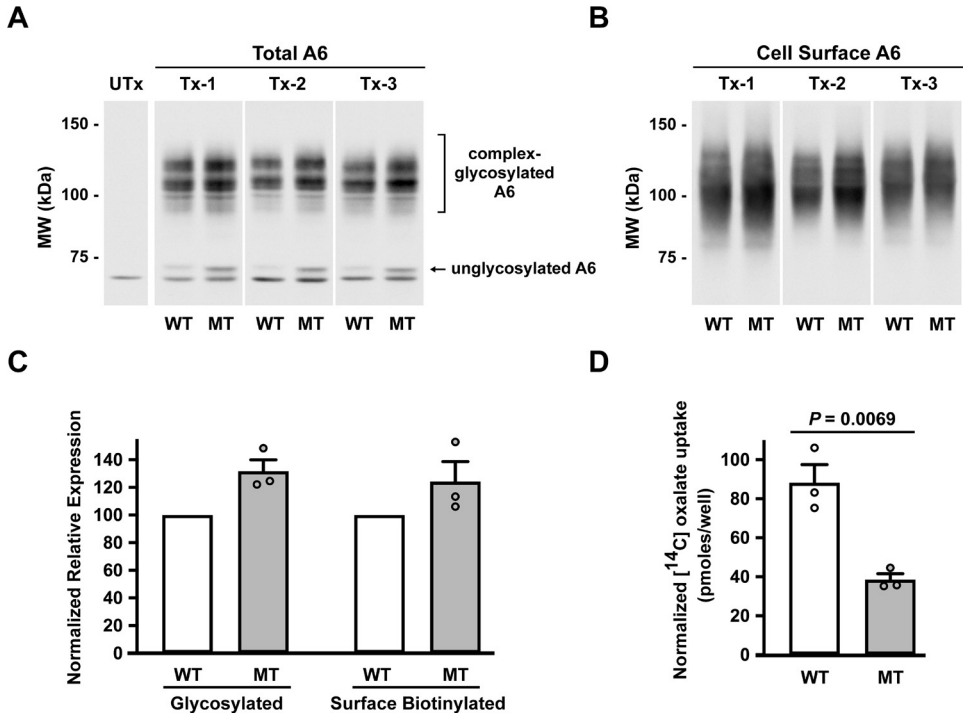

Figure 3 The R507W mutation directly impairs chloride-dependent oxalate transport capability in human SLC26A6. The initial characterisation of the Δ507 mutation suggested that the degree of inhibition of the Slc26a6-mediated chloride-dependent oxalate transport activity was significantly greater than that predicted by decreased protein expression alone. To better address that possibility, we transfected OKP cells with 2.5× more mutant (MT) than wild-type (WT) human SLC26A6 (hA6) in an effort to significantly enhance the apparent transport activity of Δ507-hA6. Cells were transfected with either 0.25 µg of HA-MT (MT) or 0.1 µg HA-WT (WT) cDNA per well of a 24-well plate. The experiments were performed and data presented identically as in panels A–C of figure 1. Panel A: western analysis of total cell lysates isolated from each transfection condition. Panel B: western analysis of cell surface biotinylatable hA6 from each transfection condition. Panel C: expression levels of total and cell surface biotinylatable hA6. Expression levels were determined by densitometry. All WT levels are expressed as 100 (%), and the individual MT values vary accordingly. Panel D: chloride-dependent ^{14}C-oxalate uptake attributable to transfected wild-type (WT; HA-WT) and mutant (MT; HA-MT) Slc26a6. The principal objective of this experiment was to directly address the transport capability of mutant relative to wild-type Slc26a6 independent of protein expression. To that end, the transport data presented in panel D were normalised to cell surface biotinylatable hA6 for each transfection. tx, transfection; Utx, untransfected.

the two constructs multimerise with wild-type SLC26A6 with a similar efficacy, their relative recoveries by coimmunoprecipitation should closely match the relative recovery of *myc*-WT in the primary immunoprecipitation for each transfection condition. The apparent decrease in coimmunoprecipitation of HA-MT relative to HA-WT observed in figure 5D and quantified in figure 5E is not significantly different to that observed for the primary immunoprecipitation of *myc*-WT observed in figure 5B when cotransfected with HA-WT versus HA-MT. This strongly suggests that the p.R507W mutation does not impair the efficacy of formation of the SLC26A6 multimeric complex per se. The demonstration of formation of MT/WT heteromultimers can explain the dominant negative effect of the MT transporter if it is misfolded, has altered stability in the plasma membrane and/or has reduced oxalate transport ability.

Identification of additional deleterious Slc26a6 mutations in cases with nl from UK Biobank

We next analysed up to 200 619 samples with available exome sequencing data in UK Biobank. Unfortunately, NL was not well recorded in the UK Biobank phenotypes as we identified 5267 patients with recorded NL that corresponds to a prevalence of 2% only. This prevalence is very far from the well-known prevalence of NL in the UK (13%).[25] Following a case-only design, we found two heterozygous protein-truncating *SLC26A6* mutations (NM_022911.3:c. 3G>A/p.Met1? and NM_022911.3:c.1132C>T/p.Gln378*) in two males. These two mutations were very rare in GnomAD (with a minor allele frequency <0.00005). Those two additional independent cases support a possible contribution of *SLC26A6* loss of function mutations to NL. Unfortunately, urinary oxalate excretion is not among the urine parameters available in the UK Biobank phenotype.

DISCUSSION

We show complementary genetic and functional evidence for a novel mechanism of inherited enteric hyperoxaluria in humans. Using a candidate gene analysis of whole-exome sequencing data, we identified a rare c.1519C>T mutation in the *SLC26A6* gene encoding an oxalate transporter in a family affected by hyperoxaluria. This mutation leads to the substitution of the arginine in position 507 by a tryptophan. Further extensive in vitro characterisation revealed that the mutation decreases both SLC26A6 transport function and membrane expression. Moreover, the mutant allele also exerts a profound dominant negative effect on the WT allele, suggesting that the mutation might affect SLC26A6-mediated oxalate secretion more than gene haploinsufficiency alone would do.

The results of our experiments demonstrating that coexpression of mutant and WT SLC26A6 decreases total and cell-surface expression of the WT protein, that mutant SLC26A6 is capable of forming multimeric structures with WT SLC26A6 and that the

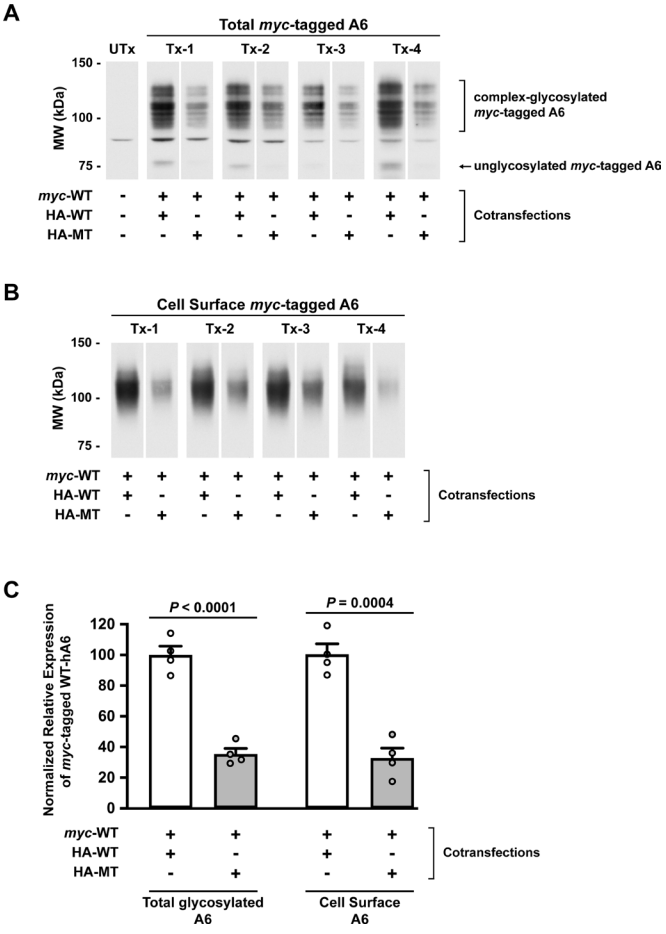

Figure 4 Coexpression of the R507W mutant significantly reduces both total and cell surface expression of wild-type SLC26A6. OKP cells were cotransfected with 0.1 µg *myc*-tagged human SLC26A6 (*myc*-WT) cDNA and either 0.1 µg HA-tagged wild-type Slc26a6 (HA-WT) cDNA or 0.25 µg HA-tagged Arg507Trp mutant Slc26a6 (HA-MT) cDNA per well of a 24-well dish. Cotransfection conditions were selected to achieve equivalent levels of expression of each HA-tagged cDNA construct to facilitate a direct comparison of the effects of coexpression of each protein. Cells were assayed 72 hours postcotransfection. See online supplemental figure S3 for a representative cotransfection experiment illustrating simultaneous expression of each epitope-tagged construct. Panel A: western analysis of *myc*-tagged wild-type Slc26a6 expression in total cell lysates isolated from each cotransfection. Panel B: western analysis of cell surface biotinylatable *myc*-tagged Slc26a6 from each cotransfection. Western blots depicted in panels A+B were probed with a mouse anti-*myc* monoclonal antibody (Thermo Fisher R950-25; 1:5000 dilution). Panel C: expression levels of total and cell surface biotinylatable *myc*-tagged Slc26a6. Expression levels were determined by densitometry. To facilitate comparisons between transfections (n=4 independent transfections) *myc*-WT:HA-MT cotransfection expression levels were expressed relative to the densitometry values for *myc*-WT:HA-WT cotransfection expression levels for each transfection and *myc*-WT:HA-WT cotransfection expression levels were normalised to a mean value of 100 (%). Co-IP, coimmunoprecipitation; Co-Tx, cotransfection; IP, immunoprecipitation; Tx, transfection; Utx, untransfected.

presence of a tryptophan in position 507 is predicted to destabilise the interaction of the mutant SLC26A6 monomer with the lipid bilayer suggest that potential mutant–mutant homodimers and mutant–wild type heterodimers are both very likely to be unstable in the cell plasma membrane. The dominant-negative effect of the mutant SLC26A6 on the wild-type protein assembled in the heterodimer (WT/MT SLC26A6) combined with the inhibitory effect of the mutation itself expressed in the homodimer (MT/MT SLC26A6) would be expected to decrease the production of functional SLC26A6 in the plasma membrane by much more than the 50% predicted by the heterozygous mutation.

SLC26A6 is an anion exchanger from the solute carrier family 26 expressed at the apical membrane of many types of epithelial cells including enterocytes in the gastrointestinal tract.[26] It can exchange intracellular oxalate for external chloride, and hence, performs apical oxalate secretion.[27] Oxalate transport across the intestinal epithelium results from the combination of passive paracellular absorption and active transcellular secretion.[28] Mouse studies have shown that SLC26A6 plays a critical role in intestinal secretion of oxalate.[12 13] Therefore, inactivation of *Slc26a6* in mice enhances net oxalate absorption, leading to higher plasma oxalate and ultimately increased urinary oxalate excretion, particularly when dietary intake of oxalate is high.[12] Our findings suggest that the c.1519C>T/p.R507W mutation in SLC26A6 may cause similar pathophysiology resulting in enteric hyperoxaluria in humans. In this regard, it is striking that the patient's hyperoxaluria was dramatically reduced by adding calcium to her diet, strongly suggesting that hyperoxaluria in her case was mostly from enteric origin and can be controlled by treatments that limit passive paracellular absorption of oxalate.

Four previous studies have assessed the possible association of *SLC26A6* mutations with hyperoxaluria and calcium oxalate urolithiasis:

In the first study, the authors screened a cohort of 94 patients with PH and 96 controls.[14] The non-synonymous *SLC26A6* variants that were detected in cases were actually frequent (minor allele frequency ≥1%) in one or more populations from the GnomAD browser (v2.1.1). A c.616G>A (p.V206M) mutant was most common (11%) and showed a 30% reduction in oxalate transport activity. However, heterozygosity for this variant did not affect plasma or urine oxalate levels in the study population. There was no significant effect of any identified variants on oxalate excretion. The p.V206M variant of *SLC26A6* was subsequently described in a second study.[15] This variant was highly frequent (minor allele frequency (MAF) ~10% in all populations). Again, this variant was not associated with urolithiasis or with hyperoxaluria. In a third study, Lu *et al*[16] functionally assessed non-synonymous *SLC26A6* variants that were listed in the public database dbSNP, according to in silico analyses. The authors found a significant association between the low-frequency (but not rare) rs184187143 variant (with a MAF of 0.4% in the Finnish population) and urolithiasis risk (unadjusted p value=0.007). However, no mechanistic insight potentially explaining this association was provided. Finally, two additional heterozygous variants of *SLC26A6* have recently been reported.[17] The first rare p.R621G variant was identified in a non-stone former individual who exhibited a normal (<40 mg/d) urinary excretion of oxalate. According to several in silico programmes (PolyPhen, SIFT, Mutation Taster, Align GVGD), this mutation was totally benign. The second rare p.D674N variant that abolished *SLC26A6* expression and Cl^--dependent bicarbonate transport when transfected in HEK cells was identified in a patient presenting with calcium oxalate urolithiasis. However, the authors did not report whether this variant was cosegregating with lithiasis in the family of the patient. Moreover, in the proband the mutation was not associated with hyperoxaluria but rather with a marked hypocitraturia, in line with previous studies from same group showing that mutation of the

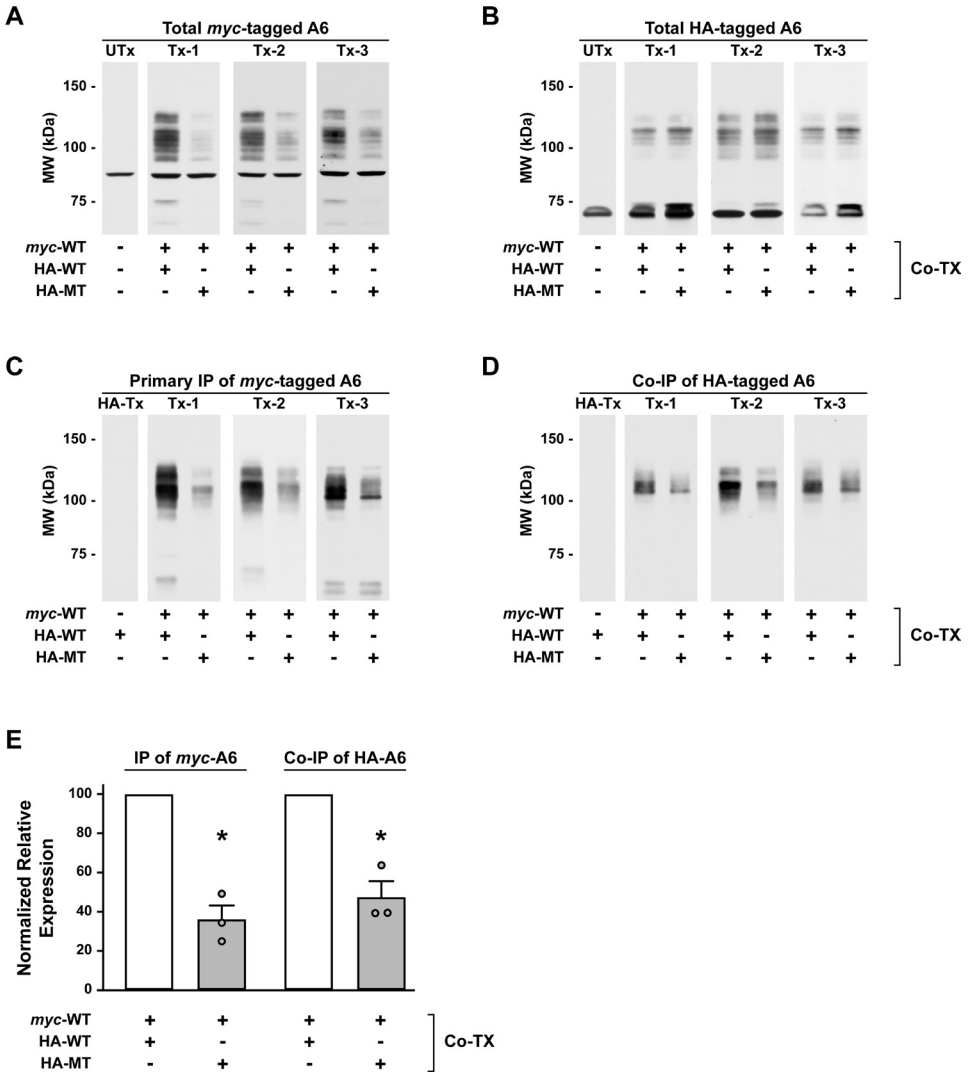

Figure 5 The R507W substitution does not inhibit association of MT-A6 with WT-A6. The principal objective of this experiment was to determine if the p.R507W mutation affected the ability of the resultant mutant to associate with wild-type (WT) Slc26a6 and form the prototypic Slc26a6 multimeric complex. By using different epitope tags for the potential binding partners, we used anti-*myc* tag (WT) primary immunoprecipitation to assess association with HA-tagged protomers (WT +MT) by monitoring levels of coimmunoprecipitation. OKP cells were cotransfected (Co-Tx) as described for figure 3, solubilised with 1% digitonin and subjected to immunoprecipitation with a mouse anti-*myc* monoclonal antibody (Thermo Fisher R950-25; 5 µg IgG/mL lysate). Panel A: western analysis of *myc*-tagged WT Slc26a6 expression in total cell lysates isolated from each cotransfection. Panel B: western analysis of HA-tagged Slc26a6 expression in total cell lysates isolated from each cotransfection. Panel C: western analysis of primary immunoprecipitated *myc*-tagged WT Slc26a6 from each cotransfection. Panel D: western analysis of coimmunoprecipitated HA-tagged Slc26a6 from each cotransfection. Western blots depicted in panels A+C were probed with anti-*myc* antibody R950-25 (1:5000 dilution) and those in panels B+D were probed with anti-HA antibody 71–5500 (1:50 dilution). Panel E: relative expression of primary immunoprecipitated *myc*-tagged WT Slc26a6 and coimmunoprecipitated HA-tagged WT or mutant Slc26a6. Expression levels were determined by densitometry. To facilitate comparisons between cotransfections (n=3 individual cotransfection events; Tx-1 to Tx-3), protein expression levels determined for the *myc*-WT/HA-MT cotransfection condition were expressed relative to the densitometry values for the *myc*-WT/HA-WT cotransfection condition for each experiment, and *myc*-WT:HA-WT cotransfection expression levels were normalised to 100 (%). *Not significantly different at p=0.3566. tx, transfection; Utx, untransfected.

STAS domain of SLC26A6 can provoke hypocitraturia, another important risk factor for NL, by altering regulation of the citrate transporter NaDC-1.[29 30] A very mild hypocitraturia, along with the marked hyperoxaluria, was also observed in our patient. It is very unlikely that such a mild decrease in urinary citrate excretion could cause such a high-frequency recurrent stone disease course, but it may have contributed along with hyperoxaluria to the increased risk for NL.

In summary, our observation that mutation p.R507W is associated with hyperoxaluria in humans supports the hypothesis that like in the mouse SLC26A6 plays a critical role in intestinal secretion of oxalate, thereby limiting net absorption of dietary oxalate. Consistent with this mechanistic hypothesis, we observed a beneficial effect of increasing calcium in the patient's diet to reduce enteric oxalate absorption and thereby urinary oxalate excretion. Accordingly, other mutations leading to defects in function of oxalate transporter SLC26A6 could be responsible for inherited form of enteric hyperoxaluria and NL in human patients. Therefore, screening for mutations in SLC26A6 should be performed in patients with hyperoxaluria in whom no mutations in the PH disease genes AGXT, or GRHPR or HOGA are

found, or in patients with enteric hyperoxaluria who have no evidence of intestinal disease.

Correction notice This article has been corrected since it was first published. The open access licence has been updated to CC BY.

Acknowledgements We would like to thank the patient and her family for their kind help and participation in the study. We would also like to thank Frédéric Allegaert and Nicolas Larcher for expert technical assistance. This research has been conducted using the UK Biobank Application #67 575.

Contributors NC, RBT, ST, BOV, SK, DWD, SB, LB, ED, EV designed, planed, and conducted experiments. All Authors analyzed and interpreted data. NC, RBT, BOV, RC, PSA and DE designed the study. BOV, RC, PSA, AB and DE wrote the manuscript. DE is the guarantor of the work.

Funding This work is funded by the National Centre for Precision Diabetic Medicine – PreciDIAB. PreciDIAB is jointly supported by the French Government under the "Investissement d'avenir" (Investments for the Future) programme managed by the "Agence Nationale de la Recherche" (ANR, French National Agency for Research) (reference: ANR-18-IBHU-0001), by the European Union through the « Fonds Européen de Développement Régional » (FEDER), by the "Conseil Régional des Hauts-de-France" (Hauts-de-France Regional Council) and by the "Métropole Européenne de Lille" (MEL, European Metropolis of Lille). This work was also supported by grants from the French National Research Agency (ANR-10-LABX-46 ((European Genomics Institute for Diabetes)) and ANR-10-EQPX-07–01 (LIGAN-PM)), from the European Research Council (ERC Reg-Seq – 715575), from FEDER and from the "Région Nord Pas-de-Calais". DE and NC are funded by grants from the foundation Philancia and from l'Association pour l'Utilisation du Rein Artificiel à la Réunion. RC is funded by grant from the French National Research Agency (ANR-16-CE14-0031-01 (PROSTARGET)). Support was also provided by NIH grant R01DK033793 to PSA. In addition, SB and LB received funding from the thematic network grant TRENAL of the Deutscher Akademischer Austauschdienst.

Competing interests None declared.

Patient consent for publication Consent obtained directly from patient(s)

Ethics approval This study involves human participants and was approved by Institutional review board of the University Hospital of La Réunion (ID :2019/CHU/10). Participants gave informed consent to participate in the study before taking part.

Provenance and peer review Not commissioned; externally peer reviewed.

Data availability statement All data relevant to the study are included in the article or uploaded as supplementary information. Not applicable.

ORCID iDs
Alaa Badreddine http://orcid.org/0000-0003-0336-4582
Peter S Aronson http://orcid.org/0000-0002-1860-2419
Dominique Eladari http://orcid.org/0000-0003-1067-0844

REFERENCES

1 Romero V, Akpinar H, Assimos DG. Kidney stones: a global picture of prevalence, incidence, and associated risk factors. *Rev Urol* 2010;12:e86–96.
2 Alexander RT, Hemmelgarn BR, Wiebe N, Bello A, Morgan C, Samuel S, Klarenbach SW, Curhan GC, Tonelli M, Alberta Kidney Disease Network. Kidney stones and kidney function loss: a cohort study. *BMJ* 2012;345:e5287. doi:10.1136/bmj.e5287
3 Denburg MR, Leonard MB, Haynes K, Tuchman S, Tasian G, Shults J, Copelovitch L. Risk of fracture in urolithiasis: a population-based cohort study using the health improvement network. *Clin J Am Soc Nephrol* 2014;9:2133–40.
4 Ferraro PM, Taylor EN, Eisner BH, Gambaro G, Rimm EB, Mukamal KJ, Curhan GC. History of kidney stones and the risk of coronary heart disease. *JAMA* 2013;310:408–15.
5 Coe FL, Evan A, Worcester E. Kidney stone disease. *J Clin Invest* 2005;115:2598–608.
6 Robertson WG, Scurr DS, Bridge CM. Factors influencing the crystallisation of calcium oxalate in urine - critique. *J Cryst Growth* 1981;53:182–94.
7 Curhan GC, Taylor EN. 24-H uric acid excretion and the risk of kidney stones. *Kidney Int* 2008;73:489–96.
8 Robertson WG, Peacock M. The cause of idiopathic calcium stone disease: hypercalciuria or hyperoxaluria? *Nephron* 1980;26:105–10.
9 Holmes RP, Goodman HO, Assimos DG. Contribution of dietary oxalate to urinary oxalate excretion. *Kidney Int* 2001;59:270–6.
10 Hagler L, Herman RH. Oxalate metabolism. I. *Am J Clin Nutr* 1973;26:758–65.
11 Cochat P, Rumsby G. Primary hyperoxaluria. *N Engl J Med* 2013;369:649–58.
12 Jiang Z, Asplin JR, Evan AP, Rajendran VM, Velazquez H, Nottoli TP, Binder HJ, Aronson PS. Calcium oxalate urolithiasis in mice lacking anion transporter Slc26a6. *Nat Genet* 2006;38:474–8.
13 Freel RW, Hatch M, Green M, Soleimani M. Ileal oxalate absorption and urinary oxalate excretion are enhanced in Slc26a6 null mice. *Am J Physiol Gastrointest Liver Physiol* 2006;290:G719–28.
14 Monico CG, Weinstein A, Jiang Z, Rohlinger AL, Cogal AG, Bjornson BB, Olson JB, Bergstralh EJ, Milliner DS, Aronson PS. Phenotypic and functional analysis of human SLC26A6 variants in patients with familial hyperoxaluria and calcium oxalate nephrolithiasis. *Am J Kidney Dis* 2008;52:1096–103.
15 Corbetta S, Eller-Vainicher C, Frigerio M, Valaperta R, Costa E, Vicentini L, Baccarelli A, Beck-Peccoz P, Spada A. Analysis of the 206M polymorphic variant of the Slc26a6 gene encoding a Cl- oxalate transporter in patients with primary hyperparathyroidism. *Eur J Endocrinol* 2009;160:283–8.
16 Lu X, Sun D, Xu B, Pan J, Wei Y, Mao X, Yu D, Liu H, Gao B. In silico screening and molecular dynamic study of nonsynonymous single nucleotide polymorphisms associated with kidney stones in the Slc26a6 gene. *J Urol* 2016;196:118–23.
17 Shimshilashvili L, Aharon S, Moe OW, Ohana E. Novel Human Polymorphisms Define a Key Role for the SLC26A6-STAS Domain in Protection From Ca^{2+}-Oxalate Lithogenesis. *Front Pharmacol* 2020;11:405.
18 Walter JD, Sawicka M, Dutzler R. Cryo-EM structures and functional characterization of murine SLC26A9 reveal mechanism of uncoupled chloride transport. *Elife* 2019;8. doi:10.7554/eLife.46986. [Epub ahead of print: 24 Jul 2019].
19 Thomson RB, Thomson CL, Aronson PS. N-glycosylation critically regulates function of oxalate transporter Slc26a6. *Am J Physiol Cell Physiol* 2016;311:C866–73.
20 Richards S, Aziz N, Bale S, Bick D, Das S, Gastier-Foster J, Grody WW, Hegde M, Lyon E, Spector E, Voelkerding K, Rehm HL, ACMG Laboratory Quality Assurance Committee. Standards and guidelines for the interpretation of sequence variants: a joint consensus recommendation of the American College of medical genetics and genomics and the association for molecular pathology. *Genet Med* 2015;17:405–24.
21 Vaser R, Adusumalli S, Leng SN, Sikic M, Ng PC, . SIFT missense predictions for genomes. *Nat Protoc* 2016;11:1–9.
22 Schwarz JM, Cooper DN, Schuelke M, Seelow D. MutationTaster2: mutation prediction for the deep-sequencing age. *Nat Methods* 2014;11:361–2.
23 Adzhubei IA, Schmidt S, Peshkin L, Ramensky VE, Gerasimova A, Bork P, Kondrashov AS, Sunyaev SR. A method and server for predicting damaging missense mutations. *Nat Methods* 2010;7:248–9.
24 Chang Y-N, Jaumann EA, Reichel K, Hartmann J, Oliver D, Hummer G, Joseph B, Geertsma ER. Structural basis for functional interactions in dimers of SLC26 transporters. *Nat Commun* 2019;10:10.
25 Heers H, Turney BW. Trends in urological stone disease: a 5-year update of hospital episode statistics. *BJU Int* 2016;118:785–9.
26 Knauf F, Yang CL, Thomson RB, Mentone SA, Giebisch G, Aronson PS. Identification of a chloride-formate exchanger expressed on the brush border membrane of renal proximal tubule cells. *Proc Natl Acad Sci U S A* 2001;98:9425–30.
27 Jiang Z, Grichtchenko II, Boron WF, Aronson PS. Specificity of anion exchange mediated by mouse Slc26a6. *J Biol Chem* 2002;277:33963–7.
28 Knauf F, Ko N, Jiang Z, Robertson WG, Van Itallie CM, Anderson JM, Aronson PS. Net intestinal transport of oxalate reflects passive absorption and SLC26A6-mediated secretion. *J Am Soc Nephrol* 2011;22:2247–55.
29 Khamaysi A, Anbtawee-Jomaa S, Fremder M, Eini-Rider H, Shimshilashvili L, Aharon S, Aizenshtein E, Shlomi T, Noguchi A, Springer D, Moe OW, Shcheynikov N, Muallem S, Ohana E. Systemic succinate homeostasis and local succinate signaling affect blood pressure and modify risks for calcium oxalate Lithogenesis. *J Am Soc Nephrol* 201910.1681/ASN.2018030277. [Epub ahead of print: 06 Feb 2019].
30 Ohana E, Shcheynikov N, Moe OW, Muallem S. Slc26A6 and NaDC-1 transporters interact to regulate oxalate and citrate homeostasis. *J Am Soc Nephrol* 2013;24:1617–26.

DETAILED METHODS

for

"Dominant negative mutation in oxalate transporter *SLC26A6* associated with enteric hyperoxaluria and nephrolithiasis" by Nicolas Cornière, R. Brent Thomson, Stéphanie Thauvin, Bruno O. Villoutreix, Sophie Karp, Diane W. Dynia, Sarah Burlein, Lennart Brinkmann, Alaa Badreddine, Aurélie Dechaume, Mehdi Derhourhi, Emmanuelle Durand, Emmanuel Vaillant, Philippe Froguel, Régine Chambrey, Peter S. Aronson, Amélie Bonnefond, & Dominique Eladari

Patients testing & ethics

Biochemical and hormone measurements were performed using standard techniques on an Alinity C auto-analyzer (Abbott Diagnostics, Rungis, France). Urinary oxalate excretion was measured by an enzymatic method using oxalate oxidase. Normal values for oxalate excretion were determined on healthy volunteers in our service and define as the lower and upper limits of the 95% confidence interval. Creatinine was measured using an isotope dilution-mass spectrometry (IDMS)-traceable enzymatic creatinine assay. Estimated GFR (eGFR) was determined using plasma creatinine value by the CKD Epidemiology Collaboration formula.[1] The relationship between parathormone (PTH) secretion and calcemia was tested using the calcium-loading test as described by Pak and Broadus.[2,3] This test also allowed assessing apparent digestive calcium absorption and net bone resorption.

All participants gave written informed consent for genetic study, and genetic testing was performed in accordance with French legislation on genetics diagnostics tests (French bioethics law no. 2004-800). The study was approved by the institutional review board of the University Hospital of La Réunion, and conducted in accordance with the Declaration of Helsinki. According to the French law, the study was declared and registered in the public database of the French National Institute of Health Data (N° MR 2105161219), and all data were collected and protected as requested by the Commission Nationale de l'Informatique et des Libertés (CNIL), collection of data was registered by the CNIL (N° 220739 v.0).

Participants from UK Biobank. We analyzed up to 200,619 samples, with available exome sequencing data. This research is part of UK Biobank research application #67575. The participants were recruited by UK Biobank from across the United

Kingdom between 13 March 2006 and 1 October 2010. People with kidney stone were defined as follows: 'at least one ICD-10 code starting with N20' (Calculus of kidney and ureter) or 'at least one ICD-10 code starting with N21' (Calculus of lower urinary tract) or 'Calculus of urinary tract in other diseases classified elsewhere' (ICD10-N22.8) or 'Unspecified renal colic' (ICD10-N23) or 'Unspecified renal colic' (ICD10-N23) or 'Other specified disorders of carbohydrate metabolism (oxaluria)' (ICD10-E748) or 'Other disorders of calcium metabolism (nephrocalcinosis)' (ICD10-E8359) or 'self-reported kidney stone' (field #20002).

DNA sequence analyses

The DNA proband was assessed through whole-exome sequencing. For this purpose, we used the Human Core Exome EF Multiplex Complete kit (Twist Bioscience) in combination with Illumina next-generation sequencing. Briefly, 50 ng DNA was fragmented through enzymatic fragmentation. The fragmented DNA samples were end-repaired, ligated to the Twist indexed adapters and purified through DNA purification beads. These samples were subsequently amplified by PCR using Illumina amplification primers and KAPA HiFi HotStart Ready mix, and purified through DNA purification beads. After size selection (between 375 bp and 425 bp) and sample quantification (Agilent BioAnalyzer), eight samples including the proband were combined in a single pool of at least 1.5 µg, and hybridized to the Twist biotin-labeled exome probes. After 16 hours at 70 °C, the hybridized targets were bound to streptavidin beads following the recommendations. After washing unspecific hybridization, the captures were subsequently amplified using the KAPA HiFi HotStart ReadyMix and quantified by both Perkin Elmer LabChip GX and Agilent BioAnalyzer. Then, the samples were sequenced on the Illumina NovaSeq 6000 system, using a paired-end 2×100 bp protocol. The demultiplexing of sequence data was performed using bcl2fastq Conversion Software v2.19.1 (Illumina). Subsequently, sequence reads were mapped to the human genome (hg38/GRCh38) using Burrows-Wheeler Aligner v0.7.17.[4] The mean depth of coverage of the target was 44.9×, with 99.08% of the target covered with more than 8 reads. The variant calling was performed using Genome Analysis ToolKit v3.8-1 (GATK).[5] Only variants with coverage higher than 8 reads were kept for further analyses. The annotation of variants was performed using the Ensembl Variant Effect Predictor tool (VEP) v100 with data from COSMIC (v90),

ClinVar (v201912), dbSNP (v153), dbNSFP (v4.0a), GENCODE (v34), gnomAD (v2.1) databases.[6]

The *SLC26A6* mutation was then confirmed in the proband, and then assessed in the family members through Sanger sequencing. Primer sequences and PCR conditions are available upon request. Fragments were sequenced in both directions, and subsequently analyzed using the 3730xl DNA Analyzer (Applied Biosystems). Electropherogram reads were assembled and examined using the SeqScape software (Applied Biosystems).

Detection of variants in UK Biobank. We used exome data from pVCF format (field #23156). Only variants with a coverage higher than 10 reads and quality GQ score higher than 20 were kept for further analyses. Annotation of variants was done using the Ensembl Variant Effect Predictor (VEP) tool version 103 (RefSeq).

SLC26A6 Expression Constructs. The generation of the HA-tagged wild-type human SLC26A6 expression construct (HA-WT) was described previously.[7] Briefly, a commercially available cDNA clone (Origene) encoding the entire transcript variant 1 isoform of human *SLC26A6* was subcloned into the retroviral mammalian expression vector pLNCX2 (Clontech). This construct was used as the template to generate the *N*-terminal HA-tagged p.R507W human SLC26A6 mutant (HA-MT) with a Q5® site-directed mutagenesis kit (New England Biolabs). The forward and reverse primers used to generate HA-MT were 5'-CGTGGTGGTCTGGACACAGAT and 5'-AGCAGCAGGGAGAAGATG respectively. HA-WT was also used as the template to develop an *N*-terminal *myc*-tagged variant (*myc*-WT). The HA-epitope tag was replaced with the *myc*-epitope tag in three steps with the Q5® site-directed mutagenesis kit with primers:

F1:5'-GAAAGATGTTCCAGATTACGCTCTGCGGAG;
R1:5'TGCTCGTCCATGGCGGCCGCCTC;
F2:5'-TCTCAGATTACGCTCTGCGGA;
R2:5'-TGAGTTTCTGCTCGTCCATGGC;
F3:5'-GATCTGCGGAGGCGAGACTAC;
R3:5'-CTCTTCTGAGATGAGTTTCTGCTCG.

PCR cycling conditions and quantities of template and primers used for each reaction were exactly as specified in the Q5® kit guidelines (New England Biolabs). HA-WT, *myc*-WT, and HA-MT were sequence validated in their entirety by the Yale Keck DNA Sequencing Facility.

Cell Culture and Transfections. OKP cells (ATTC) were utilized for all transfection experiments. They are a well characterized polarized epithelial cell line that has been used extensively to study substrate transport, protein biosynthesis, membrane trafficking, and post-translational modification of a variety of plasma membrane proteins. They are extremely amenable to standard transient transfection techniques, they do not produce significant quantities of mucus that could potentially alter efficacy of cell-surface biotinylation, and, most importantly, they do not express significant quantities of endogenous SLC26A6. OKP cells (ATTC) were maintained in high glucose DMEM (Gibco) supplemented with 2 mM L-glutamine, 1 mM sodium pyruvate, 10% FBS, and penicillin-streptomycin (100 U/ml) at 37°C in 5% CO_2. Cells were monitored routinely for mycoplasma infection by a PCR-based mycoplasma detection assay (ATTC). $1x10^5$ OKP cells per well of a 24 wells cell culture dish were reverse transiently transfected with 2 µl of Lipofectamine 2000 (Thermo Scientific) and 0.1-0.25 µg of HA-WT, *myc*-WT, or HA-MT cDNA as indicated in the respective figure legend for each experiment. Cells were assayed 72 hours post transfection.

Cell Surface Biotinylation. OKP cells were surface biotinylated 72 hours post transfection as described previously.[7] Biotinylations were performed at 4°C and all solutions were ice cold. Briefly, each well of a 24 well plate was washed 3X with complete PBS (containing 0.1 mM $CaCl_2$ and 1 mM $MgCl_2$), surface labeled with 0.25 mg of membrane impermeant EZ-Link Sulfo-NHS-LC-Biotin labeling reagent (Thermo Scientific) in a 10 mM triethanolamine buffer containing 2 mM $CaCl_2$ and 150 mM NaCl, pH 7.4 for 20 minutes (2X), washed 1X with complete PBS, washed 3X (5 minutes each) with 100 mM glycine in complete PBS to quench any unbound biotinylation reagent, washed 1X with complete PBS, and solubilized for 30 minutes at 4°C in normal salt RIPA buffer (150 mM NaCl, 50 mM Tris-HCl, 5 mM EDTA, 0.5% sodium deoxycholate, 1% Triton X-100, 0.1% SDS, pH 7.4) containing protease inhibitors (Halt; Thermo Scientific). The RIPA lysate was cleared by centrifugation at 15k x g at 4°C for 10 minutes. 10% of the cleared lysate was saved for SDS-PAGE

and the remaining fraction was incubated with Neutravidin Plus Ultralink Resin (Thermo Scientific) for 2 hours at 4°C to capture biotin-labeled surface proteins. After incubation the Neutravidin resin was washed 3X with normal salt RIPA buffer, 2X with high salt RIPA buffer (containing 500 mM NaCl) and then 2X with normal salt RIPA buffer. All washes were 10 minutes in length and performed at 4°C with ice cold wash buffers containing protease inhibitors (Halt; Thermo Scientific). Biotin-labeled proteins were eluted from the Neutravidin resin by incubation with 100°C 2X SDS-PAGE loading buffer containing 100 mm DTT for 2 minutes. The total lysate and cell-surface biotinylated fractions were subjected to standard SDS-PAGE and then transferred to a PVDF membrane (Immobilon-P, 0.45 µm; EMD Millipore) as described previously for subsequent analysis.[7] Specificity of cell surface labeling was confirmed by absence of biotin-labeling of the abundant intracellular protein, β-actin (see Supplement Figure S5).

Western analysis. PVDF membranes were probed as described previously with a rabbit anti-SLC26A6 polyclonal antibody directed against a synthetic peptide derived from the *N*-terminal region of human SLC26A6 (R29; 1:50,000 dilution),[7] a commercially available rabbit anti-HA polyclonal antibody (71-5500; 1:250 dilution; Thermo Scientific), or a commercially available mouse anti-*myc* monoclonal antibody (R950-25; 1:5000 dilution; Thermo Scientific). Primary antibody labeling was detected with either a donkey anti-rabbit or a donkey anti-mouse HRP-labeled secondary antibody (711-035-152 and 715-035-150 respectively; 1:20,000 dilution; Jackson ImmunoResearch), visualized by enhanced chemiluminescence (Clarity Western ECL Substrate; Bio-Rad), and recorded on film. R29 specificity was previously confirmed by Western analysis of duodenal lysates from wild-type and *Slc26a6*-null mice.[7] Specificity of anti-HA and anti-*myc* antibodies and validation of epitope-tagged SLC26A6 expression constructs was verified by comparative Western analysis of lysates from untransfected and HA-WT, *myc*-WT, and HA-MT transfected OKP cells.

Co-immunoprecipitation.

OKP cells were transfected as above and cultured for 72 hours prior to processing for co-immunoprecipitation. Cells were washed 3X with cold PBS and then solubilized for 1 hr with cold normal salt lysis buffer containing 50mM MOPS, 100mM NaCl, pH 7.2, 1% digitonin (Sigma D141), protease inhibitors (Roche Complete Ultra), and

phosphatase inhibitors (Roche PhosSTOP). Insoluble material was removed by centrifugation at 15k x g for 10 min at 4°C. *myc*-tagged WT SLC26A6 was immunoprecipitated by incubation with the anti-*myc* antibody R950-25 (Thermo; 5 µg IgG/ml lysate) for 2 hr at 4°C. Immunoprecipitates were captured by incubation with Protein G Sepharose Fast Flow (Sigma P3296) for 1 hr at 4°C. Sepharose beads were then washed (10 min each) at 4°C 3X with normal salt lysis buffer, 2X with high salt lysis buffer containing 500mM NaCl, and then 2X with normal salt lysis buffer. Immunoprecipitates were released from sepharose beads by incubation with 2X SDS-PAGE sample buffer containing 100mM DTT for 2 min at 100°C. The immunoprecipitates were subjected to SDS-PAGE, transferred to a PVDF membrane, and then analyzed by Western blot with antibodies directed against the HA- and *myc*-epitope tags (71-5500 and R950-25 antibodies respectively).

Cl^--dependent ^{14}C-oxalate uptake. See reference[7] for a detailed description of the rationale and methodology behind the assessment of Cl^--gradient dependent ^{14}C-oxalate uptake mediated by the SLC26A6 expression constructs (HA-WT and HA-MT) when transfected into OKP cells. Briefly, uptakes were performed for each transfection condition in the presence and absence of an outwardly directed chloride gradient to provide an estimate of the proportion of the total ^{14}C-oxalate cell uptake that was specifically chloride-dependent. Uptakes were also performed in untransfected cells (exposed to transfection reagent alone) to provide an estimate of background levels of endogenous chloride-dependent ^{14}C-oxalate uptake. The background values were then used to normalize expression of chloride-dependent ^{14}C-oxalate uptake to that directly and solely attributable to the activity of the transfected SLC26A6 expression constructs. See Suppl. Fig. S3 for a detailed example of data handling for a representative transfection event.

All uptakes were performed at room temperature and with the exception of the ice-cold Stop Buffer all uptake-related solutions were held at room temperature for the duration of each uptake experiment. Briefly, OKP cells were maintained in normal chloride high-glucose DMEM (as above) for 72 hours post transfection before each uptake experiment. Cells were washed 1X for 2 min with a chloride-free K-gluconate buffer (130 mM K-gluconate, 5 mM glucose, 20 mM HEPES, pH 7.4) to minimize residual extracellular chloride before incubating with 0.2 µCi (8 µM) ^{14}C-oxalate for 2 minutes in either the presence (200 µl K-gluconate buffer; as above) or absence (200

µl KCl buffer; 130 mM KCl, 5 mM glucose, 20 mM HEPES, pH 7.4) of an outwardly directed chloride gradient. Cell uptake of ^{14}C-oxalate was terminated by a series (3X) of 2-minute washes with ice cold K-gluconate (as above) stop buffer. The stop buffer was removed and cells were lysed by sequential 5-minute incubations of each well with 200 µl 0.1 N NaOH followed by 200 µl 0.1 N HCl. The lysate was added to 5 ml of Opti-Fluor (PerkinElmer) scintillation cocktail and counted in a Tri-Carb 2910 TR (PerkinElmer) liquid scintillation analyzer.

Statistics. For the transfection events described in Figures 1 and 2 uptakes and companion biotinylations were performed in triplicate (3 wells each condition) and spot estimates were averaged to generate a single value. Each averaged value from each transfection event represents n=1 for subsequent statistical analyses. Therefore n=3 represents 3 independent transfection events with 3 wells per transfection for each condition for both ^{14}C-oxalate uptake and cell surface biotinylation assessment. Due to the more extensive nature of the Western analysis required for the cotransfection study described in Figure 3 each value represents data obtained from a single well. Therefore n=4 represents 4 independent transfections with 1 well per transfection for each condition. Data values are presented as mean ± SEM. Statistical significance was evaluated by unpaired two-tailed Student's t-test (GraphPad Prism).

In Silico analyses of the effects of the p.R507W mutation on SLC26A6 protein

The human SLC26A6 protein sequence (Q9BXS9) was downloaded from the UniProt database.[8] Eight other sequences from different species were selected (Pan troglodytes, Rattus norvegicus, Mus musculus, Canis familiaris, Gallus gallus, Xenopus tropicalis, Tetraodon nigroviridis, and Danio rerio) in order to investigate inter-species amino acid conservation. Multiple sequence alignment was performed with Clustal Omega,[9] via the EMBL-EBI web services.[10] The Consurf server was used to obtain amino acid conservation scores within the family by comparing 150 homologous sequences.[11] A comparative model for the human SLC26A6 protein was developed using the SwissModel server, [12] and the experimental structure of the mouse Slc26a9 homodimer anion transporter was used as structural template.[13] Alternative sequence to structure alignments were investigated using the PROMALS3D server to select the final alignment to use for the modeling procedure.[14] The SLC26A6 3D model structure was geometry optimized using the PREFMD structure refinement via molecular

dynamics simulation package[15] while the analysis of the electrostatic properties was carried out with our PCE server.[16]

The human SLC26A6 3D model was inserted in a virtual membrane using the PPM server.[17] A fast estimation of the protein flexibility was performed using the PredyFlexy server that classifies amino acid residues into three class: rigid, intermediate or flexible sites.[18] The PyMOL Molecular Graphics System (Version 1.8.2.2 Schrödinger, LLC) and Chimera were both used for the interactive structural analysis.[19] The assessment of the protein stability was carried out with two different approaches DUET,[20] and SAAFEC.[21] These tools compute ΔΔG values between the wild-type and the variant proteins. The Residue Interaction Network Generator (RING) software was used to gain additional insights into the structures of the human SLC26A6 protein 3D model through visualization of non-bonded interactions.[22] The RING-2.0 server was used in our study.[23] The generated RING network XML file was then analyzed with Cytoscape.[24] Twenty-six parameters that can help predict the impact of an amino acid substitution on the structure and function of a protein were investigated using some of the above-mentioned computations and after interactive structural analysis.[25-28] To condense the resulting information into a single figure, we developed a Python script that makes use of the Matplotlib plotting library so as to generate a flower-donut traffic light chart.

Supplementary References

1. Inker LA, Schmid CH, Tighiouart H, et al. Estimating glomerular filtration rate from serum creatinine and cystatin C. N Engl J Med 2012;367:20-9.
2. Pak CY, Kaplan R, Bone H, et al. A simple test for the diagnosis of absorptive, resorptive and renal hypercalciurias. N Engl J Med 1975;292:497-500.
3. Broadus AE, Dominguez M, Bartter FC. Pathophysiological studies in idiopathic hypercalciuria: use of an oral calcium tolerance test to characterize distinctive hypercalciuric subgroups. J Clin Endocrinol Metab 1978;47:751-60.
4. Li H, Durbin R. Fast and accurate short read alignment with Burrows-Wheeler transform. Bioinformatics 2009;25:1754-60.
5. McKenna A, Hanna M, Banks E, et al. The Genome Analysis Toolkit: a MapReduce framework for analyzing next-generation DNA sequencing data. Genome Res 2010;20:1297-303.

6. McLaren W, Gil L, Hunt SE, et al. The Ensembl Variant Effect Predictor. Genome Biol 2016;17:122.
7. Thomson RB, Thomson CL, Aronson PS. N-glycosylation critically regulates function of oxalate transporter SLC26A6. Am J Physiol Cell Physiol 2016;311:C866-C73.
8. UniProt C. UniProt: a worldwide hub of protein knowledge. Nucleic Acids Res 2019;47:D506-D15.
9. Sievers F, Wilm A, Dineen D, et al. Fast, scalable generation of high-quality protein multiple sequence alignments using Clustal Omega. Mol Syst Biol 2011;7:539.
10. Madeira F, Madhusoodanan N, Lee J, et al. Using EMBL-EBI Services via Web Interface and Programmatically via Web Services. Curr Protoc Bioinformatics 2019;66:e74.
11. Ashkenazy H, Abadi S, Martz E, et al. ConSurf 2016: an improved methodology to estimate and visualize evolutionary conservation in macromolecules. Nucleic Acids Res 2016;44:W344-50.
12. Waterhouse A, Bertoni M, Bienert S, et al. SWISS-MODEL: homology modelling of protein structures and complexes. Nucleic Acids Res 2018;46:W296-W303.
13. Walter JD, Sawicka M, Dutzler R. Cryo-EM structures and functional characterization of murine Slc26a9 reveal mechanism of uncoupled chloride transport. Elife 2019;8.
14. Pei J, Grishin NV. PROMALS3D: multiple protein sequence alignment enhanced with evolutionary and three-dimensional structural information. Methods Mol Biol 2014;1079:263-71.
15. Heo L, Feig M. PREFMD: a web server for protein structure refinement via molecular dynamics simulations. Bioinformatics 2018;34:1063-65.
16. Miteva MA, Tuffery P, Villoutreix BO. PCE: web tools to compute protein continuum electrostatics. Nucleic Acids Res 2005;33:W372-5.
17. Lomize MA, Pogozheva ID, Joo H, et al. OPM database and PPM web server: resources for positioning of proteins in membranes. Nucleic Acids Res 2012;40:D370-6.
18. de Brevern AG, Bornot A, Craveur P, et al. PredyFlexy: flexibility and local structure prediction from sequence. Nucleic Acids Res 2012;40:W317-22.

19. Pettersen EF, Goddard TD, Huang CC, et al. UCSF Chimera--a visualization system for exploratory research and analysis. J Comput Chem 2004;25:1605-12.
20. Pires DE, Ascher DB, Blundell TL. DUET: a server for predicting effects of mutations on protein stability using an integrated computational approach. Nucleic Acids Res 2014;42:W314-9.
21. Getov I, Petukh M, Alexov E. SAAFEC: Predicting the Effect of Single Point Mutations on Protein Folding Free Energy Using a Knowledge-Modified MM/PBSA Approach. Int J Mol Sci 2016;17:512.
22. Martin AJ, Vidotto M, Boscariol F, et al. RING: networking interacting residues, evolutionary information and energetics in protein structures. Bioinformatics 2011;27:2003-5.
23. Piovesan D, Minervini G, Tosatto SC. The RING 2.0 web server for high quality residue interaction networks. Nucleic Acids Res 2016;44:W367-74.
24. Shannon P, Markiel A, Ozier O, et al. Cytoscape: a software environment for integrated models of biomolecular interaction networks. Genome Res 2003;13:2498-504.
25. Kucukkal TG, Petukh M, Li L, et al. Structural and physico-chemical effects of disease and non-disease nsSNPs on proteins. Curr Opin Struct Biol 2015;32:18-24.
26. Thusberg J, Vihinen M. Pathogenic or not? And if so, then how? Studying the effects of missense mutations using bioinformatics methods. Hum Mutat 2009;30:703-14.
27. Villoutreix BO. Structural bioinformatics: methods, concepts and applications to blood coagulation proteins. Curr Protein Pept Sci 2002;3:341-64.
28. Wang Z, Moult J. SNPs, protein structure, and disease. Hum Mutat 2001;17:263-70.

SUPPLEMENTARY RESULTS

for

"Dominant negative mutation in oxalate transporter *SLC26A6* associated with enteric hyperoxaluria and nephrolithiasis" by Nicolas Cornière, R. Brent Thomson, Stéphanie Thauvin, Bruno O. Villoutreix, Sophie Karp, Diane W. Dynia, Sarah Burlein, Lennart Brinkmann, Alaa Badreddine, Aurélie Dechaume, Mehdi Derhourhi, Emmanuelle Durand, Emmanuel Vaillant, Philippe Froguel, Régine Chambrey, Peter S. Aronson, Amélie Bonnefond, & Dominique Eladari

Detailed In Silico analyses of the effects of the p.R507W mutation on SLC26A6

Human SLC26A6 residue p.R507 was found fully conserved in an interspecies comparison. The conservation of this residue was also very high in this family of proteins (*i.e.,* the score at position 507 was equal to 8, the maximum is 9, via the Consurf server). We built a homology model using as experimental template the mouse Slc26a9 homodimer anion transporter 3D structure (Fig. 1). The modeling was possible as the overall sequence identity between the two proteins is around 40% (Suppl. Fig. S6). One large insertion loop in SLC26A6 could not be predicted in the STAS domain but this area is far away from position 507 (Suppl. Fig. S6, Fig. 1).

The human SLC26A6 model structure positioned into a membrane is shown in Fig. 5. p.R507 is located on the C-terminal side of the last transmembrane helix (Suppl. Fig. S6), prior to the STAS domain. This residue is essentially buried, at the interface with residues from the second subunit (Fig. 1). It makes a salt bridge with p.D682 of the other subunit, and has polar interactions with p.Q715 of the other subunit and p.N470 of the same subunit. It has also hydrophobic/aromatic contacts with p.F680 of the other subunit, which is distant from the expected Cl^- channel (Fig. 1). The region of p.R507 should be essentially rigid (PredyFlexy computation), and thus not very tolerant to the p.R507W substitution. Interactive structural analysis via PyMol and Chimera highlights that the replacement of p.R507 with a tryptophan damages the above-mentioned hydrogen bonds and salt-bridge while creating steric clashes with the surrounding amino acids.

ΔΔG stability studies (Suppl. Fig. S7), computed with DUET and SAAFEC, also underline an important change in stability suggesting that the mutant protein will be

affected as compared to the wild-type. We used the RING sever to compute a residue interaction network that we visualized in Cytoscape. Residue p.R507 is not highly connected (Suppl. Fig. S8) but many residues around make numerous non-covalent interactions with the surrounding (*e.g.*, with p.T508) and as such, the R to W is expected to alter the structure of the last helix of this domain. The clashes resulting from the p.R507W substitution together with the loss of hydrogen bonds and salt-bridge should damage this region of the mutant protein and most likely perturb correct interaction with the membrane. These data are summarized in the flower-donut-traffic-light chart presented in Suppl. Fig. S7.

SUPPLEMENTARY FIGURES &METHODS

for

"Dominant negative mutation in oxalate transporter *SLC26A6* associated with enteric hyperoxaluria and nephrolithiasis" by Nicolas Cornière, R. Brent Thomson, Stéphanie Thauvin, Bruno O. Villoutreix, Sophie Karp, Diane W. Dynia, Sarah Burlein, Lennart Brinkmann, Alaa Badreddine, Aurélie Dechaume, Mehdi Derhourhi, Emmanuelle Durand, Emmanuel Vaillant, Philippe Froguel, Régine Chambrey, Peter S. Aronson, Amélie Bonnefond, & Dominique Eladari

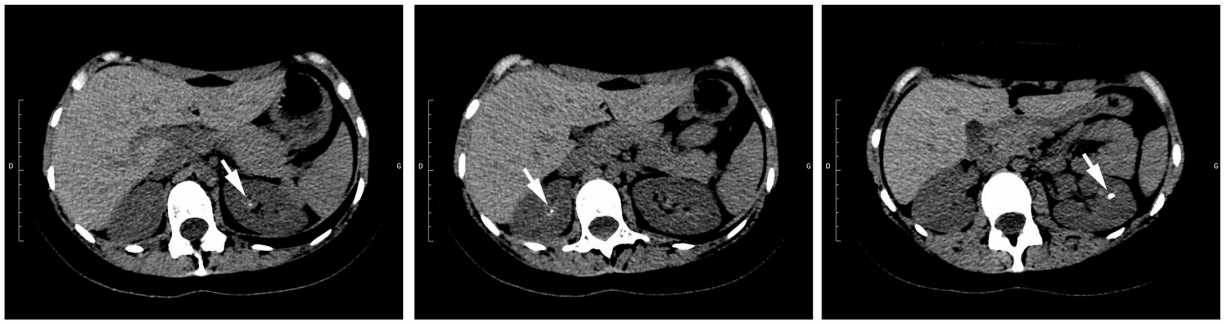

Supplemental Figure S1. Abdominal CT scan of the proband showing the presence of bilateral kidney stones. White arrows indicate the presence of kidney stones

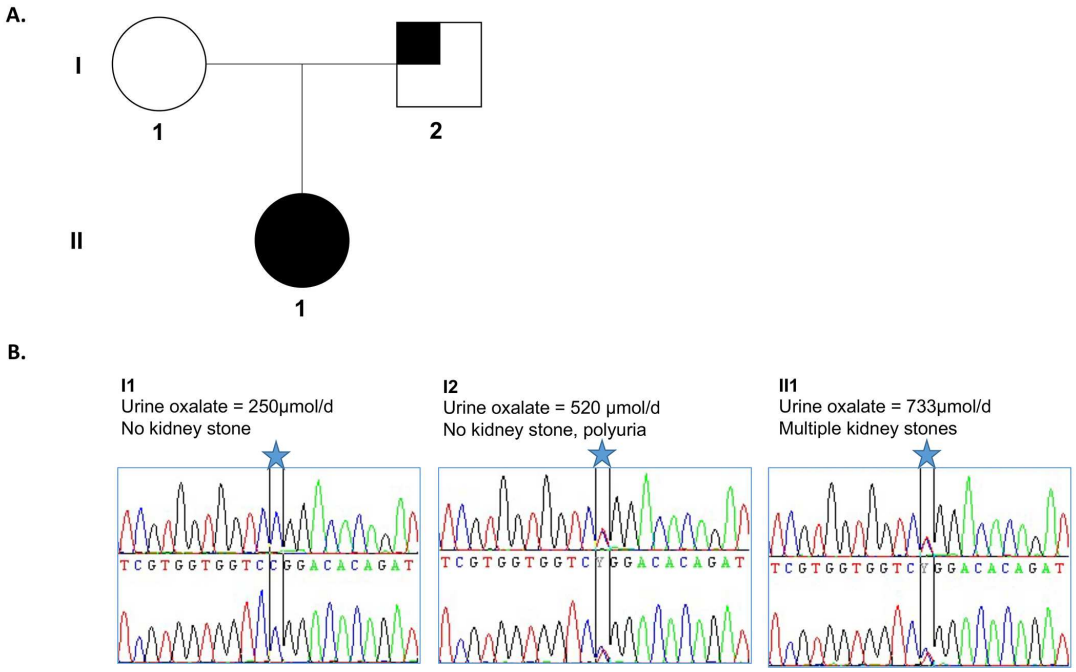

Supplemental Figure S2. Family pedigree and molecular analyses.
The pedigree of the family is illustrated panel A. Panel B, the proband (II1) carries a heterozygous c.1519C>T/p. R507W missense mutation in *SLC26A6* (NM_022911.2) that is inherited from her father (I2). The mother (I1) is wild type. The mutation is represented with a blue star in the sequencing chromatograms. Partial black shading in patient I:2 indicate the presence of isolated hyperoxaluria; full black shading of patient II:1 indicate the presence of hyperoxaluria and kidney stones.

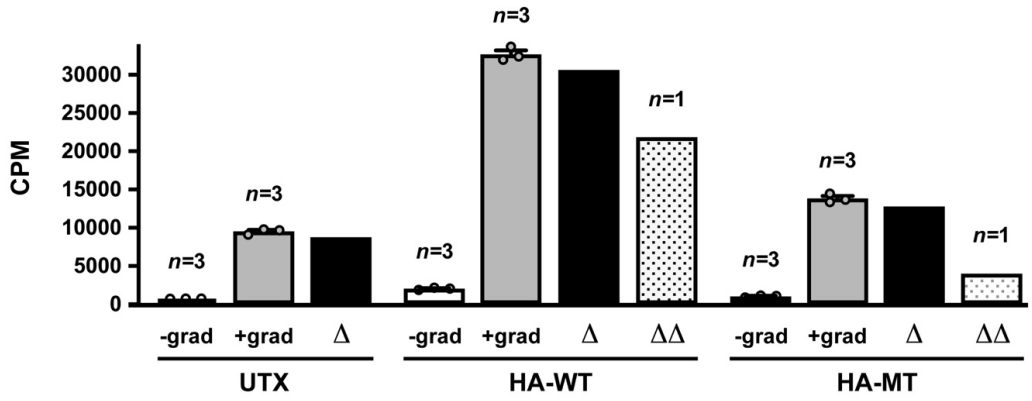

Supplemental Figure S3. Detailed description of a single representative ^{14}C-oxalate uptake experiment depicted in Figure 1. 6 wells of a 24-well plate were seeded with 1x10^5 cells per well of untransfected (UTX; transfection reagent alone), HA-WT transfected (0.1 µg cDNA per well), or HA-MT transfected (0.1 µg cDNA per well) OKP cells. For each condition ^{14}C-oxalate uptakes were performed in either the presence (+ grad; 3 wells) or absence (- grad; 3 wells) of an outwardly directed Cl^- gradient. Chloride-dependent ^{14}C-oxalate uptake was determined as the mean difference in uptake observed in the presence or absence of the imposed chloride gradient (Δ) for untransfected, wild-type SLC26A6 transfected, and mutant SLC26A6 transfected cells respectively. The component of chloride-dependent ^{14}C-oxalate uptake directly attributable to either wild-type or mutant SLC26A6 *per se* (ΔΔ) was determined by subtracting ΔUTX (endogenous chloride-dependent ^{14}C-oxalate uptake) from ΔHA-WT or ΔHA-MT respectively. This results in n = 1 for subsequent statistical analyses. CPM, counts per minute.

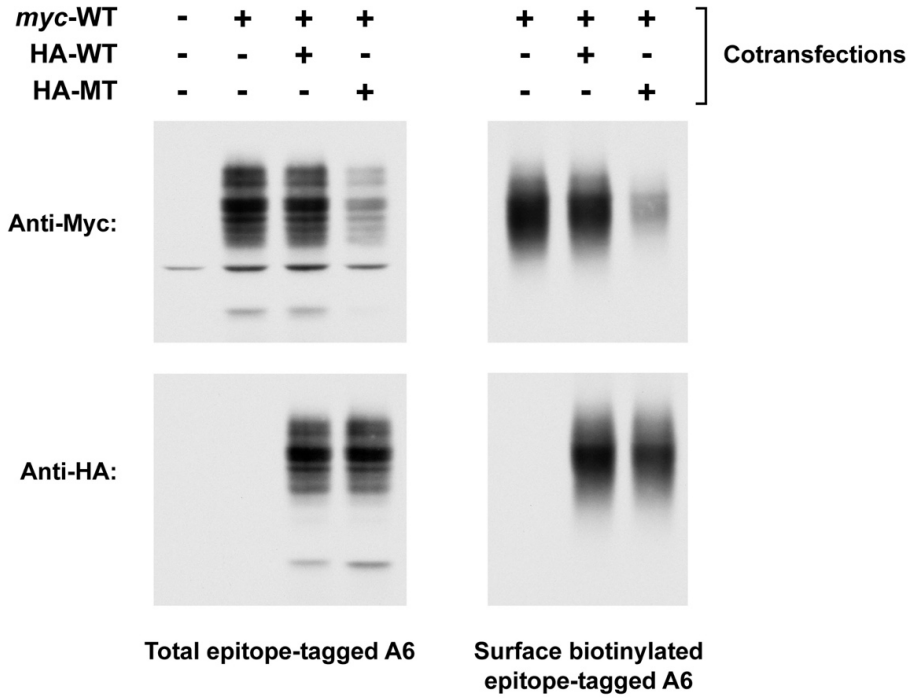

Supplemental Figure S4. Representative OKP cell cotransfection experiment depicting expression of both total and cell surface biotinylated *myc*-tagged and HA-tagged SLC26A6 expression constructs. OKP cells were cotransfected with *myc*-tagged wild-type human SLC26A6 (*myc*-WT; 0.1 µg cDNA per well) and either HA-tagged wild-type (HA-WT; 0.1 µg cDNA per well) or HA-tagged Arg507Trp mutant (HA-MT; 0.25 µg cDNA per well) human SLC26A6. Individually transfected *myc*-tagged SLC26A6 (0.1 µg cDNA per well) is included for comparison. **Upper Panels:** Western blots probed with an anti-*myc* antibody depicting expression of the *myc*-tagged wild-type SLC26A6 expression construct (*myc*-WT) under various transfection conditions. **Lower Panels:** Identical Western blots with aliquots of the same protein samples probed with an anti-HA antibody depicting expression of the HA-tagged wild-type (HA-WT) and mutant (HA-MT) SLC26A6 expression constructs under various transfection conditions.

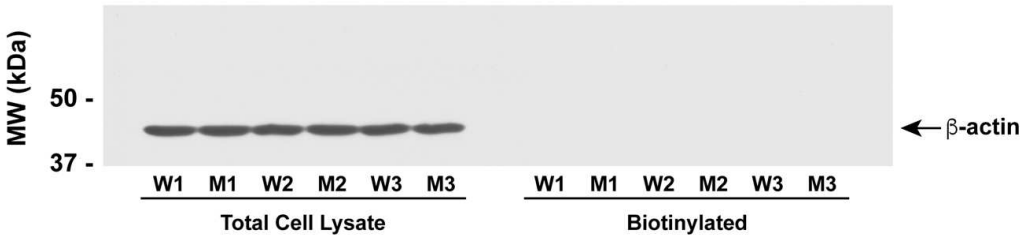

Supplement Figure S5. Specificity of cell-surface protein biotin labeling of transiently transfected OKP cells. A representative Western blot of SLC26A6 transfected OKP cells was probed with an antibody directed against the abundant intracellular protein, β-actin. Specificity of cell-surface protein biotin-labeling was confirmed by absence of β-actin staining in the biotinylated protein lanes despite evidence of high levels of β-actin expression in the total cell lysates. OKP cells were transfected with equivalent amounts (0.1 µg cDNA per well of a 24 well dish) of either wild-type (WT; HA-WT; replicates W1 to W3) or mutant (MT; HA-MT; replicates M1 to M3) human SLC26A6 cDNA. Cells were subjected to cell-surface biotinylation 72 hours post transfection. Total cell lysate lanes were loaded with 5% of the total RIPA lysate harvested from each respective well of a 24 well cell culture dish after the biotinylation reaction. Biotinylated lanes were loaded with biotin-labeled proteins isolated from 45% of the total RIPA lysate harvested from each respective well. The resulting Western blot was probed with an anti-β-actin mouse monoclonal antibody (Santa Cruz sc-69879; 1:5000 dilution).

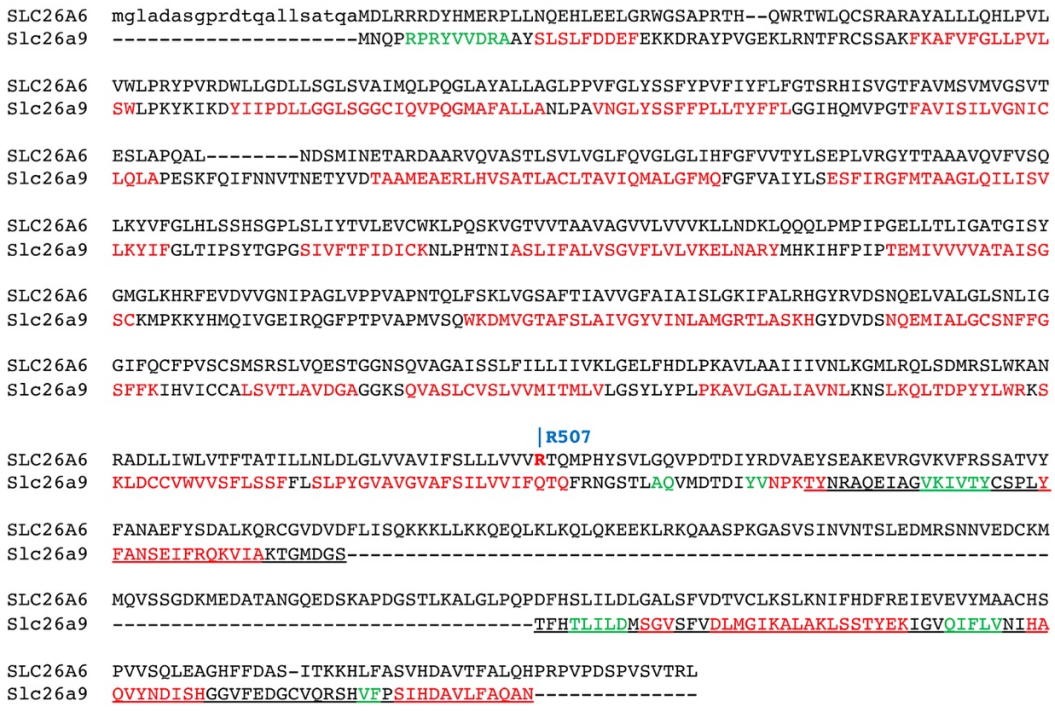

Supplementary Fig S6. Sequence and structural alignment of human SLC26A6 and mouse Slc26a9 proteins

This sequence alignment was used to build the structural model of human SLC26A6. The sequence of the human protein was aligned to the mouse Slc26a9 protein as this protein is the closest homologue with a known experimental structure. This alignment generated with PROMALS3D takes into account 3D structural information. The amino acids colored green are in beta strand structures in the mouse Slc26a9 protein while the residues in red are located in helices. The underlined residues highlight the STAS domain. Human SLC26A6 R507 is flagged. The secondary structure elements of the mouse Slc26a9 protein are expected to be highly conserved in the family, and as such, should be present in the human SLC26A6 protein. Insertions/deletions are indeed located outside these secondary structure elements, as expected in most situations. The long insertion in the human SLC26A6 protein in the STAS domain could not be predicted but as it is far away from position 507, this does not interfere with our structural analysis.

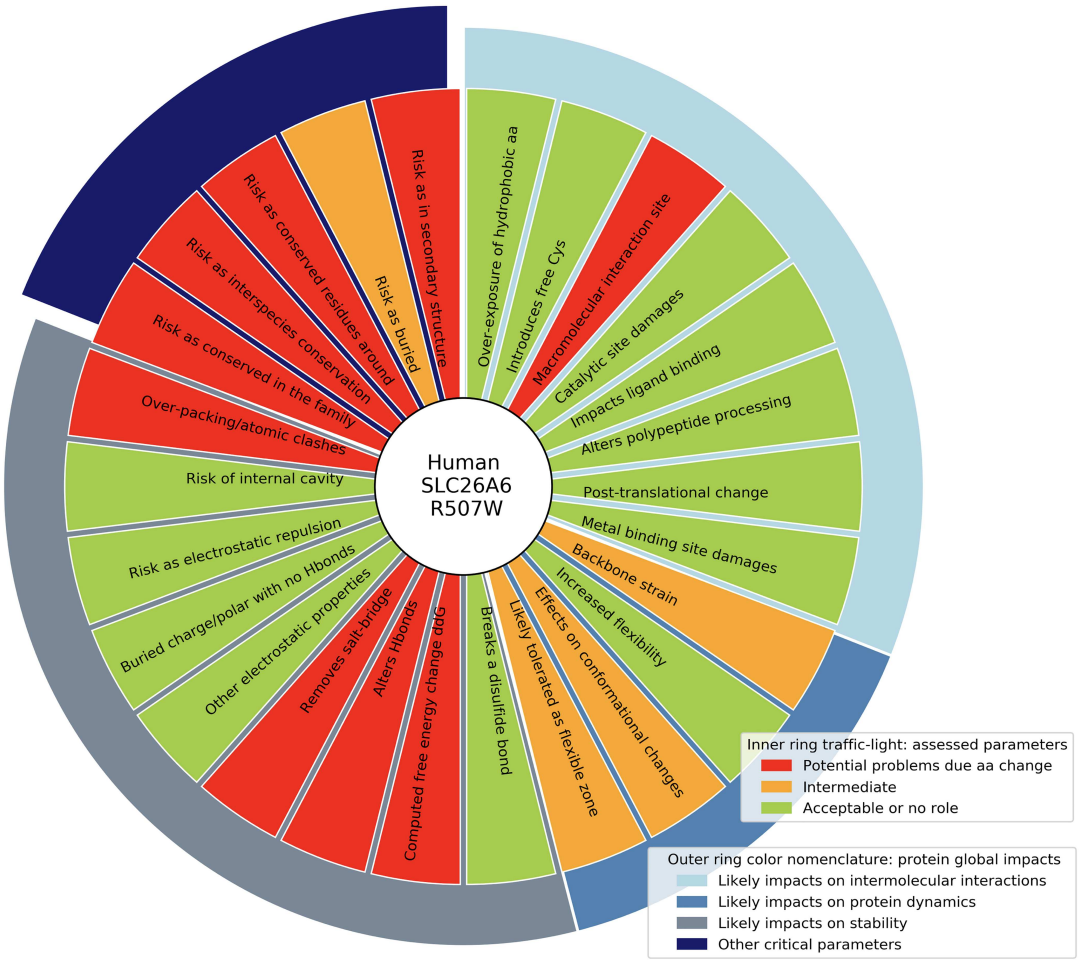

Supplemental Figure S7. R507W mutation flower-donut traffic-light chart analysis
Different parameters evaluating the impact of an amino acid substitution on the structure and function of a protein were computed. The R507W amino acid substitution has several types of predicted negative impact. These include altered intermolecular interactions (e.g., damages proper interaction of the mutant protein with the membrane), altered dynamics of the protein by forcing a large residue into a region that has not much room to accommodate such a change, and altered stability as hydrogen bonds and a salt bridge are perturbed together with the creation of numerous steric clashes with the surrounding residues. Further, the DUET predicted stability change (ΔΔG) value for the R507W mutation was found to be -0.934 kcal/mol (destabilizing), while the value computed with SAAFEC was -1.767 kcal/mol (destabilizing). Other factors important to consider when evaluating the R507W amino acid substitution are that the R residue at position 507 is overall highly conserved as are the surrounding residues, and that it is partially buried and located in an alpha-helix. Taken together, these observations suggest that a W at this position is deleterious to the normal structure and function of the protein.

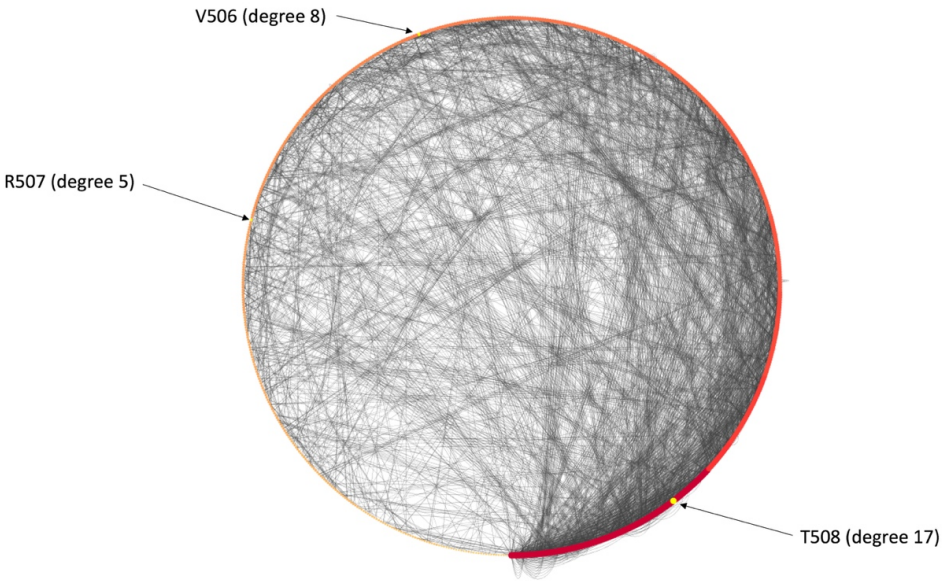

Supplemental Fig S8. SLC26A6 residues interaction networks.
Residue interaction network computation can be used to gain knowledge about a protein structure and function. In this context, amino acid residues are referred to as nodes while edges represent non-covalent interactions. Structural features can be reported for each node such as degree, here the number of non-covalent interactions with surrounding amino acids or cofactors. Intuitively, a substitution that involves a highly connected residue (non covalent interaction with its surrounding, high node degree) is likely to perturb the structure and/or the function of a protein. Here we show a degree sorted circular layout representation of the computed RING network visualized in Cytoscape (few non covalent interactions around any amino acid of the protein 3D model, small red/orange dots, towards many interactions, large red dot). The non-covalent interactions between the protein amino acids, as computed from the predicted 3D structure, are shown as grey lines and each dot on the circle represents a residue. Here, we focus on R507 (yellow dot) to illustrate the use of such visualization. This residue (node) makes only five non-covalent interactions with its surrounding (node degree = 5) but if we investigate residues that are very close to R507 (*eg.,* V506 or T508), it is seen that these residues have numerous interactions with the surrounding amino acids. The R507 to W substitution will create steric clashes and further perturb this highly connected region with most likely an impact on the structure (e.g., damage the last helix of the domain where R507 is located, a critical secondary element in this family of proteins), the stability, and the dynamics of the mutant protein.

SUPPLEMENTARY TABLE

for

"Dominant negative mutation in oxalate transporter *SLC26A6* associated with enteric hyperoxaluria and nephrolithiasis" by Nicolas Cornière, R. Brent Thomson, Stéphanie Thauvin, Bruno O. Villoutreix, Sophie Karp, Diane W. Dynia, Sarah Burlein, Lennart Brinkmann, Alaa Badreddine, Aurélie Dechaume, Mehdi Derhourhi, Emmanuelle Durand, Emmanuel Vaillant, Philippe Froguel, Régine Chambrey, Peter S. Aronson, Amélie Bonnefond, & Dominique Eladari

Supplementary Table 1. List of genes investigated in the present study

Gene ID	Gene name	NM ID	Location	Inheri-tance	Phenotype	Urolithiasis	Salt-losing nephropathy	Proximal tubulopathy
ADCY10	adenylate cyclase 10	NM_018417.5	1q24.2	candidate				
AGXT	alanine--glyoxylate and serine--pyruvate aminotransferase	NM_000030.2	2q37.3	AR	Hyperoxaluria	×		
ALPL	alkaline phosphatase, biomineralization associated	NM_000478.5	1p36.12	AD/AR	Hypophosphatasia	×		
APRT	adenine phosphoribosyltransferase	NM_000485.2	16q24.3	AR	Urolithiasis, Renal failure	×		
AQP1	aquaporin 1	NM_198098.3	7p14.3	candidate				
ATP6V0A4	ATPase H+ transporting V0 subunit a4	NM_020632.2	7q34	AR	Distal renal tubular acidosis	×		
ATP6V1B1	ATPase H+ transporting V1 subunit B1	NM_001692.3	2p13.3	AR	Renal tubular acidosis	×		
BSND	barttin CLCNK type accessory subunit beta	NM_057176.2	1p32.3	AR	Bartter syndrome		×	
CA2	carbonic anhydrase 2	NM_000067.2	8q21.2	AR	Osteopetrosis with renal tubular acidosis	×	×	×
CASR	calcium sensing receptor	NM_000388.3	3q13.33-q21.1	AD/AR	Hypocalcemia, Bartter syndrome	×	×	
CFTR	CF transmembrane conductance regulator	NM_000492.3	7q31.2	AR	Cystic fibrosis	×		
CLCN5	chloride voltage-gated channel 5	NM_000084.4	Xp11.23	XLR	Dent disease, Hypophosphatemic rickets, Nephrolithiasis, Proteinuria with hypercalciuric nephrocalcinosis	×		
CLCNKB	chloride voltage-gated channel Kb	NM_000085.4	1p36.13	AR	Bartter syndrome	×	×	
CLDN14	claudin 14	NM_144492.2	21q22.13	candidate				
CLDN16	claudin 16	NM_006580.3	3q28	AR	Hypomagnesemia, Hypercalciuria, Nephrocalcinosis	×		

CLDN19	claudin 19	NM_148960.2	1p34.2	AR	Hypomagnesemia, Renal abnormalities	×		
CYP24A1	cytochrome P450 family 24 subfamily A member 1	NM_000782.4	20q13.2	AR	Infantile hypercalcemia	×		
DMP1	dentin matrix acidic phosphoprotein 1	NM_004407.3	4q22.1	AR	Hypophosphatemic rickets	×		
ENPP1	ectonucleotide pyrophosphatase/phosphodiesterase 1	NM_006208.2	6q23.2	AR	Hypophosphatemic rickets	×		
FAM20A	FAM20A golgi associated secretory pathway pseudokinase	NM_017565.3	17q24.2	AR	Enamel-renal syndrome, Nephrocalcinosis	×		
FGF23	fibroblast growth factor 23	NM_020638.2	12p13.32	AD/AR	Hypophosphatemic rickets	×		
GRHPR	glyoxylate and hydroxypyruvate reductase	NM_012203.1	9p13.2	AR	Hyperoxaluria	×		
HNF4A	hepatocyte nuclear factor 4 alpha	NM_175914.4	20q13.12	AD	Fanconi renotubular syndrome	×		×
HOGA1	4-hydroxy-2-oxoglutarate aldolase 1	NM_138413.3	10q24.2	AR	Hyperoxaluria	×		
HPRT1	hypoxanthine phosphoribosyltransferase 1	NM_000194.2	Xq26.2-q26.3	XLR	Lesch-Nyhan syndrome	×		
INVS	inversin	NM_014425.4	9q31.1	AR	Infantile nephronophthisis	×		
KCNJ1	potassium inwardly rectifying channel subfamily J member 1	NM_000220.4	11q24.3	AR	Bartter syndrome	×	×	
NPHP1	nephrocystin 1	NM_000272.3	2q13	AR	Nephronophthisis	×		
NPHP3	nephrocystin 3	NM_153240.4	3q22.1	AD/AR	Nephronophthisis	×		
OCRL	OCRL inositol polyphosphate-5-phosphatase	NM_000276.3	Xq26.1	XLR	Dent disease, Lowe syndrome	×		
PHEX	phosphate regulating endopeptidase homolog X-linked	NM_000444.5	Xp22.11	XLD	Hypophosphatemic rickets	×		
PRPS1	phosphoribosyl pyrophosphate synthetase 1	NM_002764.3	Xq22.3	XLR	Gout, PRPS-related	×		
SLC12A1	solute carrier family 12 member 1	NM_000338.2	15q21.1	AR	Bartter syndrome	×	×	
SLC22A12	solute carrier family 22 member 12	NM_144585.3	11q13.1	AR	Renal hypouricemia	×		
SLC26A1	solute carrier family 26 member 1	NM_213613.3	4p16.3	AR	Nephrolithiasis	×		
SLC26A6	solute carrier family 26 member 6	NM_022911.2	3p21.31	candidate				
SLC2A9	solute carrier family 2 member 9	NM_020041.2	4p16.1	AD/AR	Renal hypouricemia	×		
SLC34A1	solute carrier family 34 member 1	NM_003052.4	5q35.3	AD/AR	Fanconi renotubular syndrome, Infantile hypercalcemia, Hypophosphatemic nephrolithiasis and osteoporosis	×		
SLC34A3	solute carrier family 34 member 3	NM_080877.2	9q34.3	AR	Hypophosphatemic rickets, Hypercalciuria	×		
SLC3A1	solute carrier family 3 member 1	NM_000341.3	2p21	AR	Cystinuria	×		
SLC4A1	solute carrier family 4 member 1 (Diego blood group)	NM_000342.3	17q21.31	AD/AR	Distal renal tubular acidosis	×		
SLC7A9	solute carrier family 7 member 9	NM_014270.4	19q13.11	AD/AR	Cystinuria	×		
SLC9A3R1	SLC9A3 regulator 1	NM_004252.4	17q25.1	AD	Infantile Hypercalcemia, Hypophosphatemia, Nephrolithiasis	×		

TRPV5	transient receptor potential cation channel subfamily V member 5	NM_019841.6	7q34	candidate				
TRPV6	transient receptor potential cation channel subfamily V member 6	NM_018646.5	7q34	candidate				
UMPS	uridine monophosphate synthetase	NM_000373.3	3q21.2	AR	Oroticaciduria	×		
VDR	vitamin D receptor	NM_001017535.1	12q13.11	AR	Rickets	×		
XDH	xanthine dehydrogenase	NM_000379.3	2p23.1	AR	Xanthinuria	×		

AD, autosomal dominant; ***AR***, autosomal recessive; ***XLD***, X-linked dominant; ***XLR***, X-linked recessive